



Linkage between autumn sea ice loss and ensuing spring Eurasian temperature

Shuoyi Ding^{1,2} · Bingyi Wu^{1,2}

Received: 16 March 2021 / Accepted: 5 June 2021 / Published online: 11 June 2021
© The Author(s), under exclusive licence to Springer-Verlag GmbH Germany, part of Springer Nature 2021

Abstract

This study investigated the relationship between East Siberian-Chukchi-Beaufort (EsCB) sea ice concentration (SIC) anomaly in the early autumn (September–October, SO) and northern Eurasian surface temperature (Ts) variability in the early spring (March–April, MA). Results reveal that the early autumn sea ice decrease in the EsCB Seas excites an Arctic anticyclonic anomaly in the lower troposphere in the early spring, leading to cold anomalies over central Russia. The mean temperature over central Russia drops by nearly 0.8 °C, and the probability of cold anomalies increases by about 30% when the EsCB SIC reduces by one standard deviation. As responses to SO EsCB sea ice loss, atmospheric anomalies of the planetary wave 2 dominate the Arctic since October–November (ON) and are in phase with the climatological mean in the troposphere. This in-phase resonance produces much more wave energy propagating into the lower stratosphere and generates an EP flux convergence anomaly in December–January (DJ), then decelerating the zonal westerly winds. One month later (January–February, JF), the attenuation of the polar vortex reaches the peak and propagates downward into the troposphere in the next 2 months with two major branches. One branch is located in Greenland and induces a zonal wave train from the North Atlantic to eastern Eurasia. Another branch is to maintain the anticyclonic anomaly in low-level over the Arctic. This configuration of atmospheric circulation anomalies provides favorable conditions for the southward invasion of Arctic cold air and makes northern Eurasia experience a colder early spring.

Keywords Sea ice loss · Spring northern Eurasian cooling · CAM4 sensitive experiment

1 Introduction

As an integral component of the Earth's climate system, Arctic sea ice can regulate the local atmospheric circulation, temperature and precipitation through altering the heat and momentum exchange between the atmosphere and ice-covered ocean (Serreze et al. 2007; Budikova 2009; Vihma 2014; Gao et al. 2015; Cohen et al. 2020). Meanwhile, the climate impacts of Arctic sea ice variability further expands into the mid-low latitudes by the effects of several physical pathways, including atmospheric wave bridge in the upper

troposphere (Dethloff et al. 2006), the mid-latitude synoptic eddy-mean flow interaction (Deser et al. 2000; Jaiser et al. 2012), the stratosphere-troposphere coupling involving anomalous vertical propagation of quasi-stationary planetary waves (Chen and Wu 2018; Zhang et al. 2018a, b). In recent decades, Arctic sea ice concentration (SIC) or extent presents an increasing decline rate, concurrent with a rapid warming signal and enhanced precipitation in the Arctic region (e.g., Deser et al. 2010; Screen and Simmonds 2010). Therefore, the possible impacts of Arctic sea ice anomalies in autumn or winter on the mid-high latitudinal climate variability in the subsequent seasons, especially the linkage between sea ice loss and winter continental cooling (Wu et al. 1999, 2011a, b; Francis et al. 2009; Honda et al. 2009; Petoukhov and Semenov 2010; Inoue et al. 2012; Jaiser et al. 2012; Chen et al. 2014; Mori et al. 2015, 2019; Nakamura et al. 2015; Zhang et al. 2018a, b; Ding et al. 2021; Overland et al. 2021), has received intensive scientific attention.

The previous studies have pointed out that the melting of winter pan-Arctic sea ice corresponds to a negative Arctic

✉ Bingyi Wu
bywu@fudan.edu.cn

¹ Department of Atmospheric and Oceanic Sciences and Institute of Atmospheric Sciences & CMA-FDU Joint Laboratory of Marine Meteorology, Fudan University, Shanghai 200438, China

² CMA-FDU Joint Laboratory of Marine Meteorology, Shanghai 200438, China

Oscillation/North Atlantic Oscillation (AO/NAO) (Alexander et al. 2004; Deser et al. 2004; Magnusdottir et al. 2004), but this relationship is suggested to be insignificant in some modeling studies (Singarayer et al. 2005; Blackport and Kushner 2017; Ogawa et al. 2018). Some research further discussed whether the regional sea ice anomalies in winter influence climate change in the Northern Hemispheric continent. They have found that the Barents-Kara Seas is a key region, and its sea ice decrease will induce an increased blocking and significant cooling over northern Eurasia in the wintertime (Mori et al. 2015, 2019; Li et al. 2021) via a southeastward quasi-stationary planetary wave train (Honda et al. 2009; Xu et al. 2021) or downward propagation of anomalous stratospheric signals (Zhang et al. 2018a, b; Xu et al. 2021). In addition, sea ice decrease in the Greenland Sea affected surface temperature variability over eastern North America and northern Europe (Cohen et al. 2018; Vihma et al. 2020), while sea ice decrease in the Chukchi–East Siberian Seas favored central North American cooling (Kug et al. 2015; Overland and Wang 2018).

Besides the contemporaneous correlation, several investigators attempted to explore whether the preceding autumn sea ice can be considered as a precursor for winter atmospheric circulation variability and extreme weather/climate events (Francis et al. 2009; Wu et al. 2011a, b, 2013, 2017; Francis and Vavrus 2012, 2015; Hopsch et al. 2012; Jaiser et al. 2012; Tang et al. 2013; Chen et al. 2014; Nakamura et al. 2015; Chen et al. 2021; Ding et al. 2021). Francis et al. (2009) discovered that the anomalous signals of September Arctic sea ice can be remembered by the following winter atmospheric pattern, that is, less Arctic sea ice corresponds to a “wavier” circulation and more frequent extreme weather (Francis and Vavrus 2012, 2015). Wu et al. (2011a, b) also suggested that the September SIC is a potential precursor for the intensity of winter Siberian high due to their evident negative correlation. In virtue of statistical analysis and numerical simulation, many studies pointed out that less autumn SIC in the eastern Arctic Ocean and Siberian marginal seas will make northern Eurasia or even East Asia experience significant cooling and more frequent cold-air outbreaks (Tang et al. 2013; Wu et al. 2013, 2017), accompanied by an enhanced Siberian High (Wu et al. 2011a, b), a stronger northern mode of East Asian winter monsoon (EAWM) (Chen et al. 2014) and the southward energy propagation of low-frequency waves (Gu et al. 2018). However, this relationship is non-stationary and may be modulated by summer initial atmospheric conditions (Wu et al. 2017).

Recently, some studies have focused on the climate impacts of regional sea ice variability in autumn because the atmospheric responses in the mid-high latitudes are sensitive to the geographical location of Arctic sea ice anomalies (Rinke et al. 2013; Pedersen et al. 2016; Chen et al. 2016b; Screen 2017; Cohen et al. 2020). The early

autumn SIC interannual variability was controlled by two major EOF modes and reflected notable regional differences (Deser and Teng 2013; Ding et al. 2021). Most studies have emphasized that sea ice decrease in the Barents-Kara-Laptev (BKL) Seas (see the second EOF early autumn SIC variability in Ding et al., 2021) effectively affects the large-scale atmospheric circulation (Honda et al. 2009; Wu et al. 2011a, b; Jaiser et al. 2012; Hopsch et al. 2012; Chen et al. 2016b; Screen 2017), while only a few studies analyzed the possible climate responses to the sea ice decrease in the East Siberian–Chukchi–Beaufort (EsCB) Seas (the first EOF; Chen et al. 2016b; Screen 2017; Chen and Wu 2018; Ding et al. 2021). Ding et al. (2021) found an increasingly larger amplitude of interannual variation of early autumn EsCB SIC, and pointed out that the reduced sea ice will induce an Arctic anticyclonic anomaly and evident central-western Eurasian cooling in the early winter through enhanced upward propagation of quasi-stationary planetary waves in the mid-high latitudes and associated upper tropospheric Eliassen–Palm (EP) flux convergence anomaly.

Many previous works have focused on analyzing the possible impacts and mechanism of Arctic sea ice anomalies on the winter climate variability over Eurasia. And this climate influence can even persist until spring (Wu et al. 2016; Chen and Wu 2018). Wu et al. (2016) discovered that winter sea ice loss in the Norwegian Sea and the Barents would generate a cyclonic anomaly over the Mongolian plateau by exciting a downstream propagating Rossby wave train, which accelerates the East Asian subtropical westerly jet and favors sufficient spring precipitation over East Asia. Based on the leading mode of spring Eurasian surface air temperature (SAT) anomalies, Chen and Wu (2018) revealed that the decrease (increase) of Arctic SIC over the Laptev-East Siberian-Beaufort Seas in the preceding autumn generally induces Eurasian SAT cooling (warming) in the mid-high latitudes through the modulation of Arctic Oscillation (AO) associated atmospheric circulation variations. This cross-seasonal influence is intimately connected with the interaction between the upper troposphere and lower stratosphere. Similar anomalous stratospheric signals were also observed by Ding et al. (2021). When the early autumn EsCB sea ice reduces, much more quasi-stationary planetary wave energy propagates into the lower stratosphere and attenuates the polar vortex in the wintertime, portending that the tropospheric atmospheric circulation will be again disturbed in the following months.

This study will further investigate whether the early autumn sea ice in the EsCB Seas will affect the spring climate change (surface temperature) over Eurasia at the interannual time scale and explore associated physical processes, such as the contribution of distinct planetary waves to the weakened polar vortex and downward propagation of stratospheric anomalies. This may provide another possible

predictor for spring climate change over Eurasia besides El Niño—Southern Oscillation (ENSO; Wu et al. 2010; Graf and Zanchettin 2012; Ding et al. 2017, 2018), North Atlantic sea surface temperature anomalies (Wu et al. 2011a, b), snow cover over northern Eurasia (Wu et al. 2014; Ye et al. 2015; Wu and Chen 2016) and Arctic Oscillation/North Atlantic Oscillation (AO/NAO; Miyazaki and Yasunari 2008; Zveryaev and Gulev 2009; Ionita et al. 2012; Kim and Ahn 2012; Chen et al. 2013; Song and Wu 2019a).

The structure of this manuscript is organized as follows. The reanalysis datasets, analysis methods and model description are described in Sect. 2. Section 3 displays the impacts of the early autumn sea ice anomaly in the EsCB Seas on the early spring climate (surface temperature) over Eurasia and its associated atmospheric anomalies. Section 4 further illustrates the possible physical processes for this cross-seasonal relationship involving the role of a stratospheric pathway based on the statistical diagnose and sensitive experiments. Discussion and the summary of results are provided in Sects. 5 and 6, respectively.

2 Data and methodology

Atmospheric monthly mean variables are provided by the National Center(s) for Environmental Prediction (NCEP)—U.S. Department of Energy (DOE) Reanalysis II with a resolution of $2.5^\circ \times 2.5^\circ$, including air temperature, geopotential height and horizontal winds (Kanamitsu et al. 2002). The monthly mean sea ice concentration (SIC) is derived from the Met Office Hadley Center, showing $1^\circ \times 1^\circ$ longitude/latitude resolution (Rayner et al. 2003). The overlapping period of all datasets extends from January 1979 to December 2018. Since the main focus of this study is on the interannual variability, a 9-year high pass filter was applied to all variables to remove the trend and interdecadal component.

Area-mean SIC anomalies in the region of 70.5° – 82.5° N, 135.5° E– 119.5° W, multiplying by -1, is defined as an index to depict the EsCB sea ice variations (Fig. 1a). Based on this SIC index, linear regression and correlation analyses are employed to explore the linkage between early spring climate change over Eurasia and the preceding early autumn sea ice anomaly in the EsCB Seas. The composite maps of difference between low and high SIC years, selected by a criterion of $\pm 0.8\sigma$ for the normalized EsCB index (low sea ice: 1990, 1993, 1995, 1998, 2003, 2007, 2012; high sea ice: 1992, 1994, 1996, 2001, 2006, 2009, 2013), are used for validation of the regression results. This criterion optimally compromises both small sample and signal-to-noise ratio. The significance of statistical analyses is examined by a two-tailed nonparametric Monte Carlo bootstrap significance test (Mudelsee 2010). For linear regression or correlation analysis of two-time series X and Y , their average and standard

deviation are calculated to generate 1000 sets of random numbers conforming to the normal distribution. Then, 1000 regression or correlation coefficients are obtained and sorted in ascending order. Similarly, for the difference between categories A and B, the bootstrapping procedure generates 1000 composite value through randomly selecting m and n years from $m+n$ years, and their difference is sorted in ascending order. Here, m (n) is the number of selected cases in category A (B). If the regression (correlation) coefficient and composite difference value are higher than 95% or lower than 5% of the bootstrapping estimates, it is regarded as passing through the 90% confidence level.

The horizontal propagation of planetary waves is diagnosed by horizontal wave activity flux, and the associated formulation in the log-pressure coordinate is Takaya and Nakamura (1997, 2001)

$$W = \frac{1}{2|\bar{U}|} \left\{ \begin{array}{l} \bar{u}(\overline{\psi_x'^2} - \overline{\psi' \psi_{xx}'}) + \bar{v}(\overline{\psi_x' \psi_y'} - \overline{\psi' \psi_{xy}'}) \\ \bar{u}(\overline{\psi_x' \psi_y'} - \overline{\psi' \psi_{xy}'}) + \bar{v}(\overline{\psi_y'^2} - \overline{\psi' \psi_{yy}'}) \end{array} \right\},$$

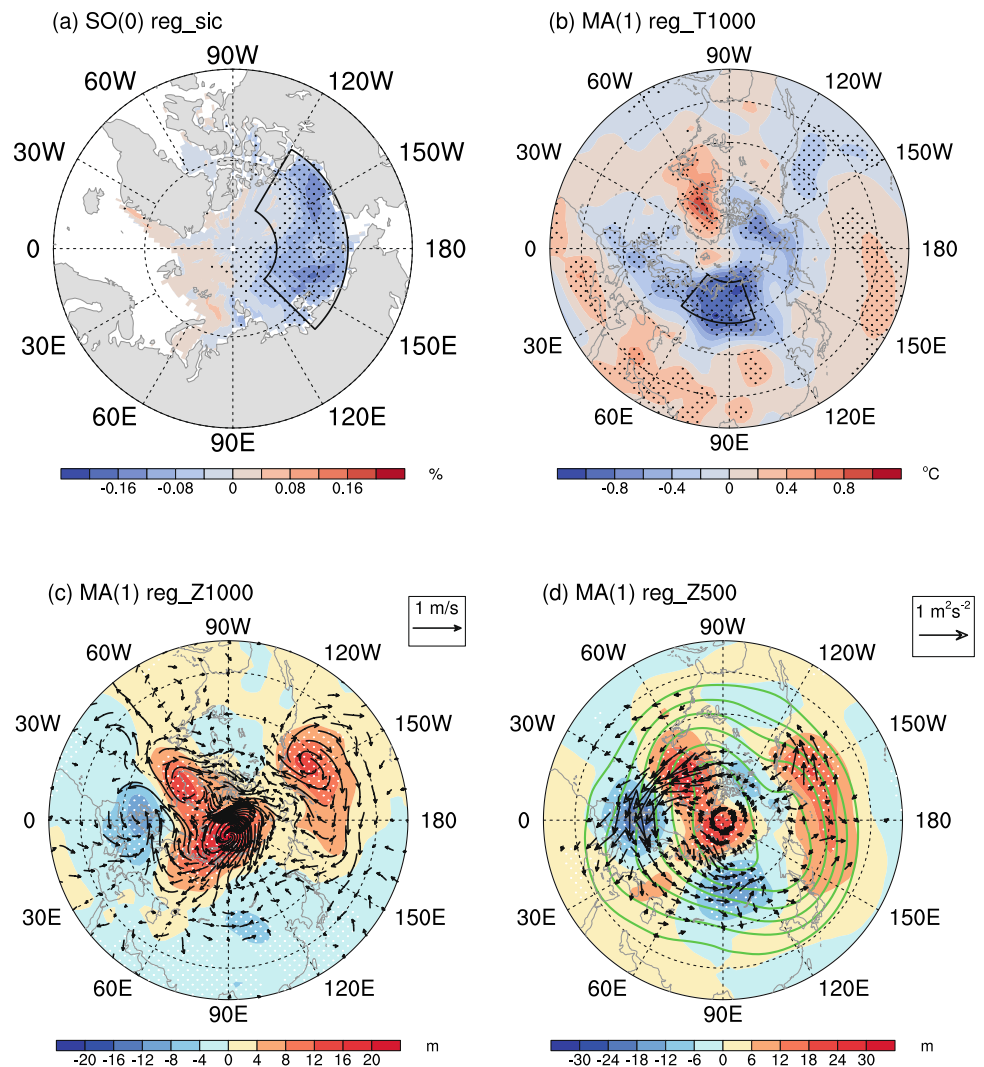
where ψ' , u and v are the perturbed geostrophic stream function, the zonal and meridional wind velocities, respectively. The overbar represents the climatological mean and the subscripts x (y) indicates the partial derivatives in the zonal (meridional) directions. In addition, we use EP flux to describe the vertical propagation characteristics of planetary wave activity (Plumb 1985; Andrews et al. 1987). The components of EP flux (\vec{F}) and its divergence (D_F) are calculated as follows:

$$F_y = -\rho a \cos \varphi \overline{\varphi u' v'}, \quad F_z = \rho a \cos \varphi \frac{Rf}{HN^2} \overline{v' T'}, \quad D_F = \frac{\nabla \cdot \vec{F}}{\rho a \cos \varphi}.$$

Here, ρ is air density, a is the radius of the earth, φ is the latitude, R is the gas constant, f is the Coriolis parameter, H is the scale height, N is buoyancy frequency, u is zonal wind, v is meridional wind and T is temperature. The primes (overbar) denotes zonal deviation (average). The EP flux divergence can portray the eddy forcing of the zonal mean flow, that is anomalous convergence (divergence) of EP flux decelerates (accelerates) the westerly winds (Edmon et al. 1980; Chen et al. 2002, 2003).

The Community Atmosphere Model version 4 (CAM4) (Neale et al. 2010) is utilized in this study to operate the sea-ice sensitivity experiments. SIC and SST from Hadley Center are specified as boundary conditions. The simulation configuration shows a horizontal resolution of 2.5° in longitude and 1.9° in latitude, and 26 vertical levels extending up to 2.2 hPa with finite volume dynamic core. Two experiments are designed to assess the impacts of early autumn EsCB sea ice decrease on the subsequent

Fig. 1 Regressed **a** early autumn (September–October; SO) SIC anomaly (shading; unit: %), **b** early spring (March–April; MA) Ts anomaly (shading; unit: °C), **c** MA geopotential height (shading; unit: m) and horizontal winds anomalies (vector; unit: m s^{-1}) at 1000 hPa and **d** MA geopotential height anomaly (shading; unit: m) and horizontal wave activity flux (vector; unit: $\text{m}^2 \text{s}^{-1}$) at 500 hPa upon normalized SO EsCB index at the interannual time scale. Green Contours in **(d)** are the climatological mean of 500 hPa geopotential height. Dots for shadings indicate the 90% confidence level. Vectors in **(c, d)** only depict the part exceeding 0.05 m s^{-1} and $0.1 \text{ m}^2 \text{ s}^{-1}$, respectively



early spring atmospheric circulation. The control experiment is run for 50 years, forced by the climatological mean of monthly SIC and SST. Note that the climatology is calculated as the mean of 1983–2012 from the Hadley Centre. The sensitivity experiment is performed with perturbed EsCB sea ice from August to October but with the same SST boundary condition as in the control experiment. Perturbed sea ice is the combination of climatological sea ice plus the EsCB sea ice decrease derived from regression of Arctic SIC upon normalized SO EsCB index. The sensitivity experiment integrates for 80 years to obtain sufficient sample sizes. The simulated results since the 11th year in two experiments are selected for calculation as the first 10 years are discarded as spin up (Zhang et al. 2018b; Nakamura et al. 2019). The atmospheric responses to the prescribed EsCB sea ice loss are defined as the difference of the ensemble mean between the sensitivity experiment and control experiment.

3 Impacts of autumn EsCB SIC on spring Eurasian temperature

To explore whether there exists a statistical correlation between spring surface temperature over Eurasia and early autumn sea ice in the EsCB Seas, the regressed air temperature (Ts) and geopotential height (Z1000) anomalies at 1000 hPa from March to May upon the normalized September–October (SO) EsCB index is first examined (not shown). Significant anomalous signals mainly occur in March and April. Therefore, this study focuses on early spring (March–April, MA) surface temperature variability linking to early autumn EsCB sea ice anomalies at the interannual time scale.

Figure 1 shows the regression of early autumn SIC anomaly and associated early spring atmospheric anomalies (1000 hPa air temperature, 1000 hPa geopotential height and horizontal winds, 500 hPa geopotential height and horizontal wave activity flux), derived from the normalized SO EsCB

index. When the SO EsCB sea ice reduces (Fig. 1a), positive geopotential height anomaly covers the Arctic regions and extends southward into western Russia (30°–60° E) in the subsequent early spring (Fig. 1c). Northerly wind anomaly to east of 30° E (Fig. 1c) favors Arctic cold air penetrating northern Eurasia and contributes to significant cooling with anomalous center around central Russia (Fig. 1b). Negative Ts anomaly also expands into northeastern China following the further southward intrusion of weak northerly wind anomaly. A positive geopotential height anomaly and significant local warming can be found over Greenland. Negative geopotential height anomaly covers the eastern North Atlantic-Europe, which favors an eastward intrusion of northeasterly wind anomaly into western Europe and induces a colder early spring there. By contrast, southern Eurasia experiences a warmer condition except for eastern China. In the middle troposphere (500 hPa), mid-high atmospheric anomalies at 500 hPa correspond well to that in the lower troposphere, indicating a quasi-barotropic structure (Fig. 1d). Alternating anticyclonic, cyclonic, anticyclonic, and cyclonic anomalies are located in Greenland, the eastern North Atlantic-western Europe, the Ural Mountains, and central Russia, respectively. It constitutes an eastward propagating quasi-stationary planetary wave train from North Atlantic to northern Eurasia. Significant negative geopotential height anomaly over central Russia indicates the deepening of the trough there (green contours), providing a favorable condition for the southward penetration of Arctic cold air. To its north, positive geopotential height anomaly in the eastern Arctic Ocean and Eurasian marginal seas also contributes to the central Russian cyclonic anomaly by the local synoptic eddy-mean flow interaction (not shown).

Considering that significant cooling mainly occurs in central Russia (57.5° N–75.0° N, 50° E–110° E), we further plot the time series of regional averaged Ts anomalies (Fig. 2), denoted as T_RUS index. This index is negatively correlated with the EsCB index at the interannual time scale ($r = -0.50$, significant at 90% confidence level), suggesting that the EsCB sea ice variability would explain 25% variation of central Russian Ts. In addition, another anticyclonic anomaly covers the North Pacific from low-level to high-level. Unlike the typical negative Arctic Oscillation (AO) pattern associated with autumn Arctic sea ice loss (Chen and Wu 2018), the whole tropospheric anomalies manifest a negative NAO signal and a weakened Aleutian low, which exhibits large similarity to the atmospheric configuration during the low SIC period as mentioned by Jaiser et al. (2013) and Wu et al. (2015). We also examine the statistical co-variability between early autumn SIC and early spring Z1000 or Ts based on singular value decomposition (SVD) analyses. The leading SVD mode also shows approximately identical characteristics to the regressed results, including sea ice loss in the EsCB Seas, Arctic anticyclonic anomaly,

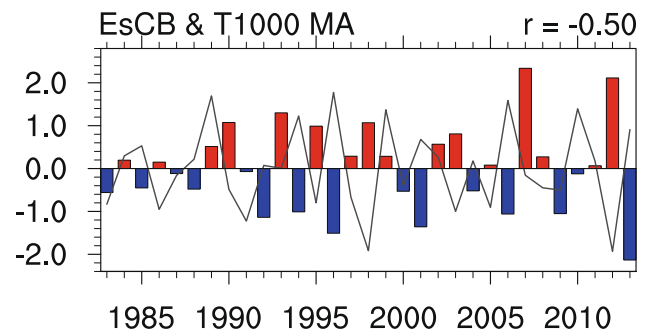


Fig. 2 Normalized time series of early spring (MA) area-mean Ts anomaly (black solid line) in central Russia (57.5°–75.0° N, 50°–110° E) at the interannual time scale. The bar graph represents normalized interannual EsCB index

zonal propagating wave train from Greenland to central Russia, and evident cooling over northern Eurasia (not shown). Thus, the above significant correlation linking early spring Eurasian climate variability to early autumn sea ice anomalies will not change by utilizing distinct statistical methods.

The sea-ice sensitivity experiments well reproduce the early spring Eurasian atmospheric and climate anomalies that are statistically related to the early autumn EsCB sea ice decrease in the observations. Figure 3 displays the surface temperature anomaly, the histogram plot of T_RUS indexes, and 1000 hPa and 500 hPa geopotential height anomalies in the early spring. Significant cooling dominates central Russia and extends southeastward to northeastern China, accompanied by a warmer condition over Greenland (Fig. 3a). Compared to the observed Ts anomalies (Fig. 1b), the cold anomaly shifts eastward and penetrates northeast China while the warm anomaly is relatively weaker. Over central Russia, the occurrence frequency of the cold conditions (less than -0.5 °C) is 59.4% (41 cases), twice as large as that of warm conditions (greater than 0.5 °C) (Fig. 3b). Especially for the extreme cold conditions (less than -2.5 °C), its occurrence frequency is twice higher than that of extreme warm conditions (greater than 2.5 °C). Therefore, as a response to less autumn EsCB sea ice, central Russia has a higher probability of experiencing a colder early spring. The corresponding lower tropospheric atmospheric configuration is featured by significant positive geopotential height anomaly over the Arctic region with a southward extension around western Russia (Fig. 3c), contributing to the evident cooling around central Russia. To its south, in the North Atlantic sector, a negative geopotential height anomaly covers the North Atlantic-western Europe and is west of the observed location (Fig. 1c), partly explaining non-significant cooling in western Europe. This deviation from the observations is accompanied by a weaker positive geopotential height anomaly over Greenland, which may be related to the simulation ability of the North Atlantic storm track. In the

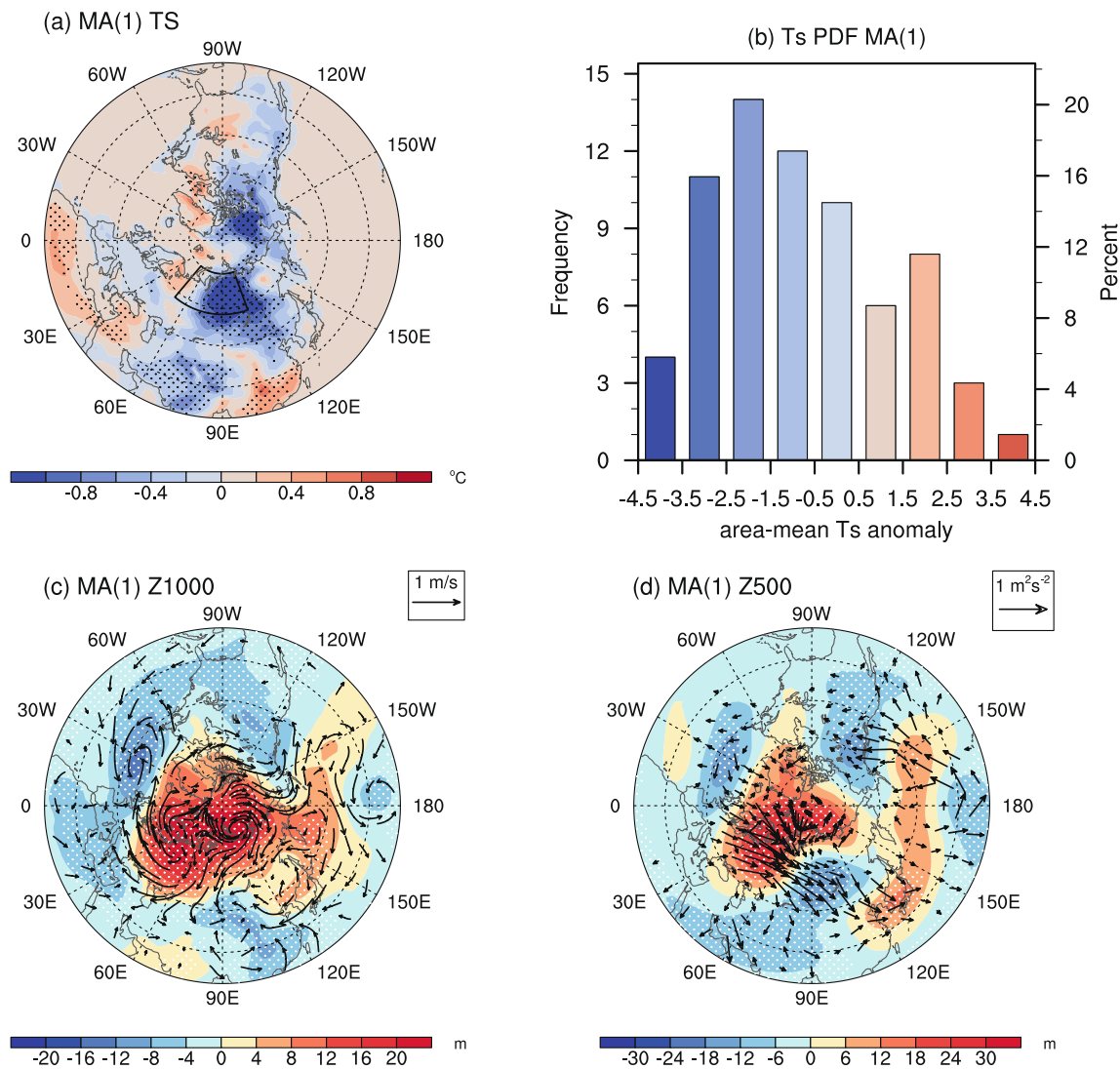


Fig. 3 Simulated MA **a** Ts anomaly (shading; unit: °C), **c** geopotential height anomaly (shading; unit: m) at 1000 hPa and **d** geopotential height anomaly (shading; unit: m) and horizontal wave activity flux (vector; unit: $\text{m}^2 \text{s}^{-1}$) at 500 hPa between sensitivity and control

experiments. **b** Histograms of T_RUS index (area-mean Ts anomaly in central Russia) in 69 early springs. Dots for shadings indicate the 90% confidence level. Vectors in **(d)** only depict the part exceeding $0.1 \text{ m}^2 \text{ s}^{-1}$

middle troposphere, eastward propagating quasi-stationary planetary waves from the North Atlantic is analogous to the observed zonal wave train, passing through the Ural Mountains and resulting in the enhanced trough over central Russia (Fig. 3d). Unlike the observations, there is no evident horizontal wave activity propagating from Greenland to the eastern North Atlantic due to a weaker anticyclonic anomaly around Greenland. Additionally, over the North Pacific, a positive geopotential height anomaly can also be detected in the model results but is much weaker and shifts westward and poleward. This may be attributed to the lack of air–sea coupling or interaction in climate models.

Both statistical and model results manifest the prominent cross-seasonal influences of early autumn EsCB sea

ice anomaly on the subsequent early spring Eurasian surface temperature variability though there exists a certain deviation from the observations. Another key question is to illustrate the possible physical pathway or mechanism linking the above cross-seasonal relation, which will be discussed in detail in Sect. 4.

4 Possible physical linkage: the role of stratospheric pathway

Many investigators have pointed out that the perturbation of the lower stratosphere can modulate the underlying tropospheric anomalies through the downward propagation of

anomalous signals associated with the barotropic effects (Ambaum and Hoskins 2002; Castanheira et al. 2009; Graf et al. 2014; Song and Wu 2019b), and the alteration of upper-level wind shear as well as the jet's latitudinal position (Scaife et al. 2012; Garfinkel et al. 2013; Graf et al. 2014). The associated effects of stratospheric anomalies will persist for several months due to its long decorrelation time of at least up to 2 months (Baldwin and Dunkerton 2001), which provides a possible pathway for autumn sea ice to influence the Eurasian climate in the subsequent seasons. Therefore, the stratospheric polar vortex may exert a crucial role in bridging the EsCB sea ice loss in the early autumn to the persistent Arctic anticyclonic anomaly in the early spring, as enlightened by previous studies (Cohen et al. 2007; Orsolini et al. 2012; King et al. 2015; Zhang et al. 2018a, b).

Accompanied by the early autumn EsCB sea ice decrease, significant weakening of stratospheric polar vortex covers the whole Arctic Ocean in DJ (December–January). It reaches the peak value and moves toward the Greenland–Eurasian sector in JF (January–February) and then gradually attenuates in the next two months (not shown). The spatial pattern in the evolution of the weakened polar vortex is approximately consistent with the regressed results of the normalized T_RUS index, especially for lower stratospheric

anomalies in DJ and JF. The DJ or JF stratospheric polar vortex (SPV) index, at the interannual time scale, is not only positively correlated with EsCB index ($r=0.31, 0.29$) but is also negatively correlated with T_RUS index ($r=-0.40, -0.57$), passing through 90% confidence level. Note that the SPV index is defined as area-mean geopotential height anomaly at 50 hPa to the north of 70°N . These significant correlation coefficients indicate that the weakened winter stratospheric polar vortex may be a crucial bridge connecting EsCB sea ice loss in the early autumn with central Russian cooling in the early spring, consistent with the results of Ding et al. (2021).

The evolution of zonal mean geopotential height anomalies (averaged over $70^\circ\text{--}90^\circ\text{N}$) and zonal mean U-wind anomalies (averaged over $60^\circ\text{--}80^\circ\text{N}$) obtained by regression upon on the normalized SO EsCB index also confirm the above statistical relationship. The strongest stratospheric signals of positive geopotential height anomaly (Fig. 4a) and decelerated westerly winds (Fig. 4b) occur in winter. These anomalies persist for at least 2 months in the lower stratosphere (Baldwin and Dunkerton 2001) and propagate downward into the troposphere, which may contribute to the re-enhancement of Arctic anticyclonic anomaly in the early spring. Much more evident downward propagations

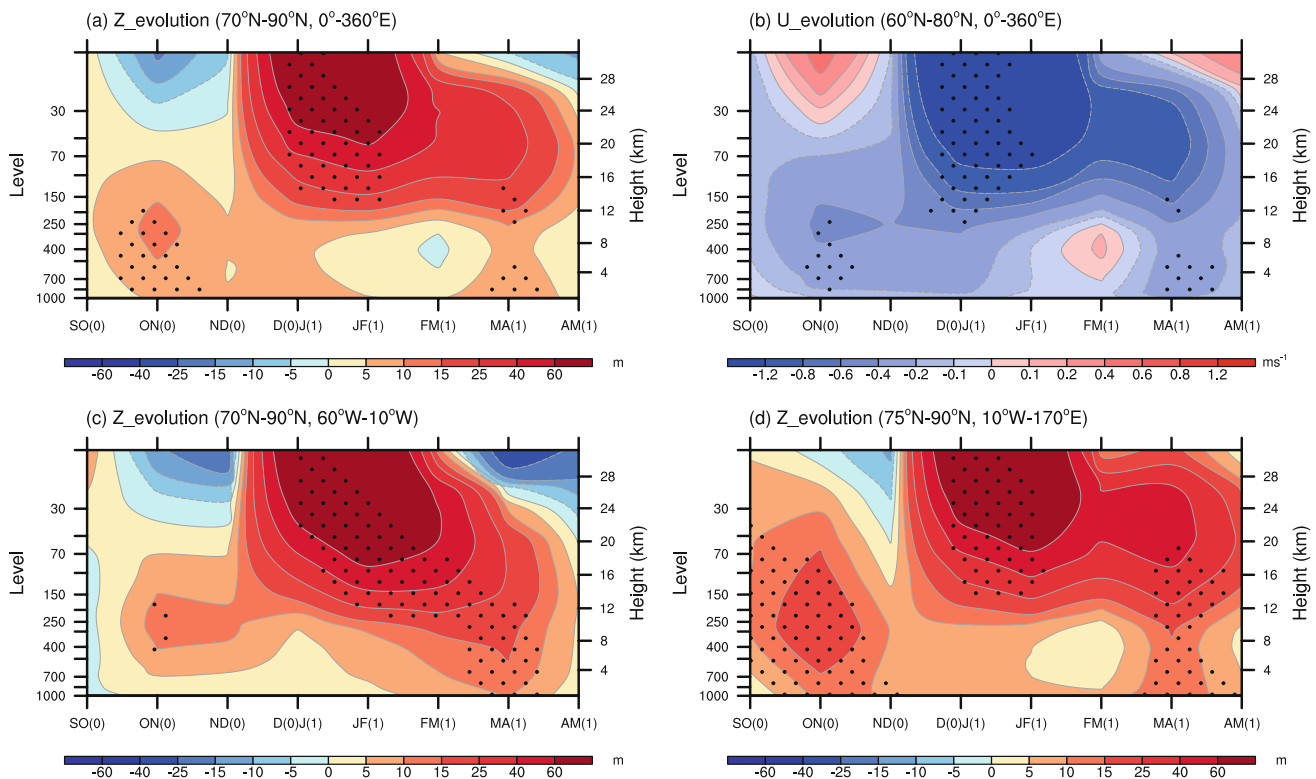


Fig. 4 Time-height cross sections of **a** area-mean geopotential height anomalies (shading; unit: m) over the Arctic region ($70^\circ\text{--}90^\circ\text{N}$, $0^\circ\text{--}360^\circ$) and **(b)** area-mean U-wind anomalies (shadings; unit: m s^{-1}) in the mid-high latitudes ($60^\circ\text{--}80^\circ\text{N}$, $0^\circ\text{--}360^\circ$) regressing on

upon normalized SO EsCB index. **c, d** as in (–), but for the area-mean geopotential height anomalies over the Greenland ($70^\circ\text{--}90^\circ\text{N}$, $60^\circ\text{--}10^\circ\text{W}$) and eastern Arctic Ocean ($75^\circ\text{--}90^\circ\text{N}$, $10^\circ\text{--}170^\circ\text{E}$), respectively. Dots for shadings indicate the 90% confidence level

are detected in two local regions. One is over Greenland (70° – 90° N, 60 – 10° W), where significant positive geopotential height anomaly propagates downward from the middle stratosphere since JF and reaches the lower troposphere 2 months later (Fig. 4c). This downward propagation will strengthen the anticyclonic anomaly around Greenland. Then, eastward propagating horizontal wave train is excited and further develops downstream into eastern Eurasia, forming a zonal wave train and deepening the trough over central Russia (Fig. 1d). Another downward propagation appears in the eastern Arctic Ocean (75° – 90° N, 10° W– 170° E), featured by positive geopotential height anomaly maintaining in the lower stratosphere for 2 months and then abruptly penetrating the troposphere in MA (Fig. 4d). This may partly explain the persistent Arctic anticyclonic anomaly until the early spring. Model results also exhibit similar downward propagating characteristics of stratospheric anomalies, as shown in Fig. 5. The weakened polar vortex in the lower stratosphere reaches the peak value in JF, then propagates downward in the next 2 months and disturbs the Arctic tropospheric circulation in MA (Fig. 5a, b). Two apparent downward propagations are located in Greenland (Fig. 5c) and the eastern Arctic Ocean (Fig. 5d), respectively.

To estimate the contribution of SO EsCB sea ice decrease to MA central Russian cooling as well as the bridging role of winter stratospheric polar vortex, we employ a Generalized

Extreme Value (GEV) distribution (Coles 2001; Michailidis and Stoev 2012) to calculate the probability density function (PDF) and cumulative distribution function (CDF) of MA T_RUS index and JF SPV index in both sensitivity and control experiments. Compared to the control experiment, the PDFs of two indexes in the sensitivity experiment show an evident shift, with the T_RUS index shifting toward the negative value (Fig. 6a) and the SPV index shifting toward the positive value (Fig. 6c). The PDFs in two experiments are significantly separated based on a Monte Carlo bootstrapping technique (Efron and Tibshirani 1994). This confirms a crucial role of SO EsCB sea ice in the Eurasian climate variability, which is manifested by a 0.8°C drop in the mean temperature of central Russia in MA and a 60gpm rise in the mean geopotential height (50 hPa) of the Arctic region in JF. Estimated by CDF, the occurrence probability of central Russian cooling in the sensitivity experiment increases by about 30% than the control experiment (Fig. 6b), close to the increased percentage (25%) in the occurrence probability of a weakened stratospheric polar vortex (Fig. 6d). It reveals that the reduced EsCB sea ice in the early autumn significantly facilitates increase in the occurrence probability of colder events around central Russia in the early spring, and the above cross-seasonal influence is realized by attenuating the winter stratospheric polar vortex.

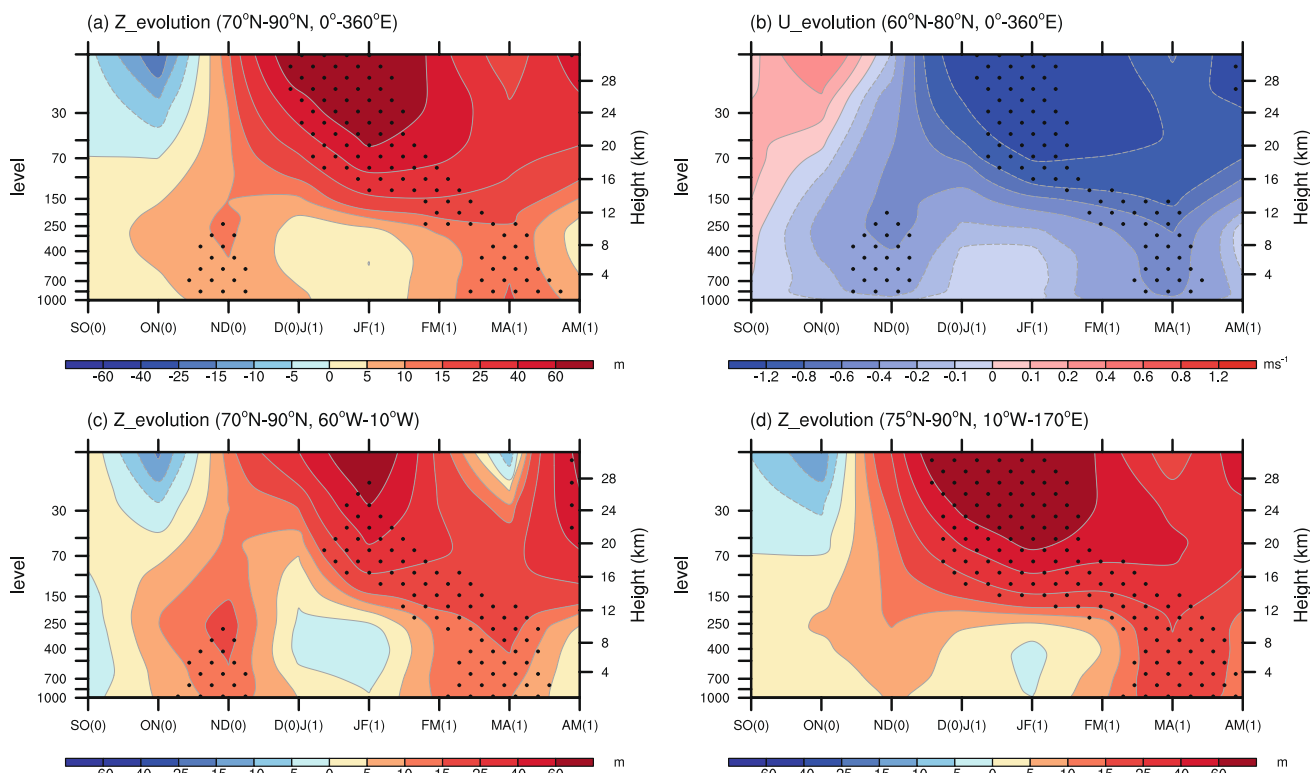


Fig. 5 As in Fig. 4, but for the simulated results between sensitivity and control experiments

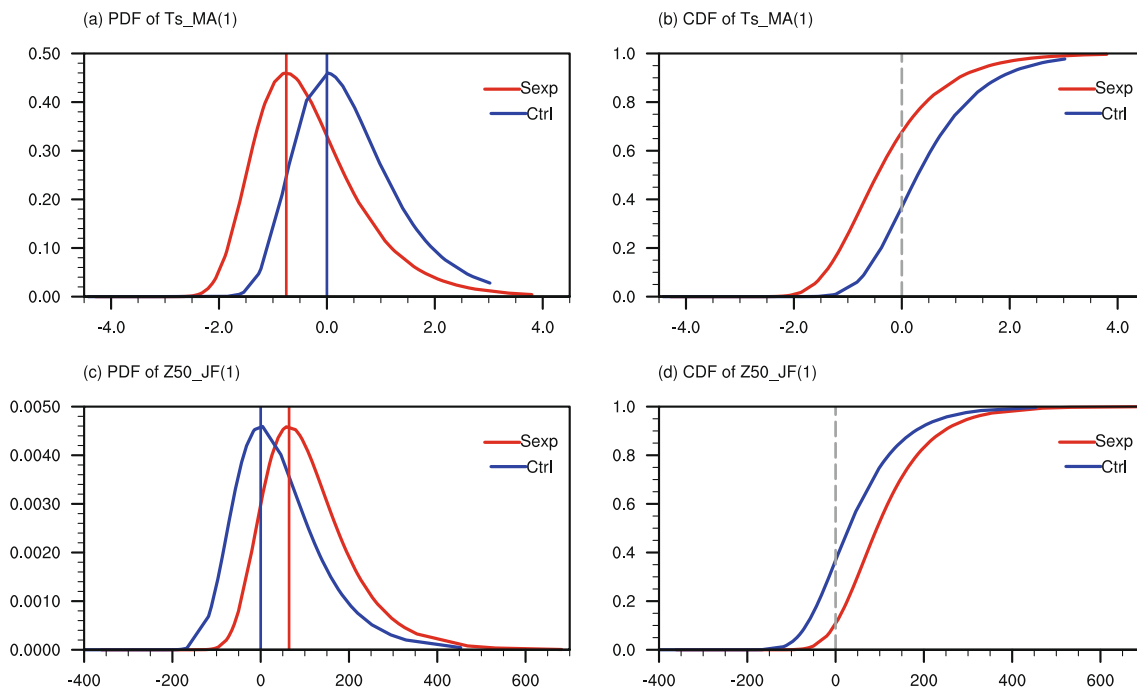


Fig. 6 **a** PDF (probability density function) and **b** CDF (cumulative distribution function) of MA T-RUS index. **c, d** As in **(a, b)**, but for the JF (January–February) SPV index

Several investigators have discovered that when autumn Arctic sea ice reduces, Arctic warm anomaly and the decreased meridional temperature gradient provide a favorable condition (decelerated westerly winds) for more quasi-stationary planetary waves propagating into the stratosphere and the associated generation of EP flux convergence anomaly, which leads to the weakening of winter stratospheric polar vortex (Chen and Wu 2018; Zhang et al. 2018a, b; Ding et al. 2021). Here, we further estimate the contribution of planetary waves with distinct wavenumber. Analogous to Ding et al. (2021), when SO EsCB sea ice reduces by one interannual standard deviation, both the observed and model results display that the strongest anomalous upward propagation of EP flux and associated stratospheric EP flux convergence anomaly appear in DJ (Fig. 7a, d), 1 month earlier than the mature phase of the weakened polar vortex (Figs. 4, 5). In the lower stratosphere of high latitudes (100–30 hPa, 60° N–80° N), the formation of EP flux convergence anomaly mainly originates from the contribution of planetary wave 2 (Fig. 7c, f). By contrast, planetary wave 1 can propagate to above 30 hPa (higher than 24 km), and its contribution is confined to the polar region (Fig. 7b, e). The area-mean EP flux convergence anomaly in the lower stratosphere (100–30 hPa, 60°–80° N) is calculated to compare the contribution of planetary waves 1 and 2 roughly. Planetary wave 2 plays a dominant role in the attenuation of the lower stratospheric polar vortex associated with the EsCB

sea ice decrease (Fig. 8), which is quite different from the main contribution achieved by planetary wave 1 when the sea ice reduces in the Barents-Kara Seas (Zhang et al. 2018b). Considering that the role of planetary wave 3 is limited, the resulting EP flux anomaly and its convergence anomaly are not shown.

Another issue worth discussing is the possible reason for the enhanced upward propagation of quasi-stationary planetary waves. In DJ, the geopotential height anomalies of planetary wave 2 are in phase with its climatological mean, especially north of 60°N (Fig. 9b, d). This will induce more wave energy to be transported into the lower stratosphere, in line with the anomalous upward EP flux in the high latitudes (Fig. 7c, f). The increased amplitude of planetary wave 2 is observed to the north of 60° N (Fig. 10b, d) and can better clarify the resonance in the 500 hPa geopotential height anomaly, indicating that more wave energy is upward transported in the Arctic region. Similar signals of an increase in the amplitude can be observed 1 or 2 months earlier (not shown). As for planetary wave 1, the in-phase resonance (Fig. 9a, c) and increased amplitude (Fig. 10a, c) are located in the mid-latitudes to the south of 60° N and induce more wave energy (anomalous upward EP flux) penetrating through the tropopause into the stratosphere at approximately 50° N (Fig. 8b, e). In a word, enhanced wave energy due to the in-phase resonance of planetary waves in the troposphere provides a possible explanation for anomalous upward EP flux.

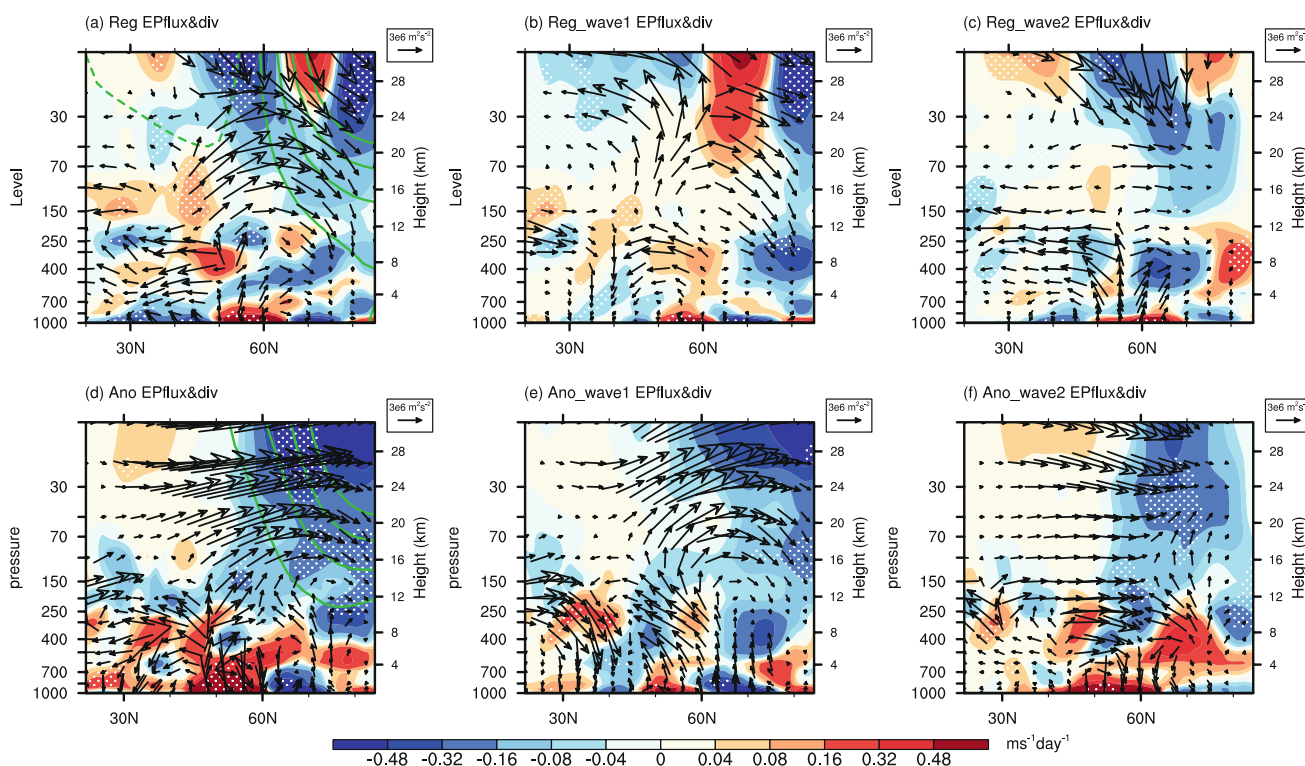


Fig. 7 Regressed DJ (December–January) zonal mean EP flux (vector; unit: $\text{m}^2 \text{s}^{-2}$), EP flux divergence (shadings; unit: $\text{m s}^{-1} \text{day}^{-1}$) and geopotential height anomalies (contour; interval: $-10, 10, 30, 50, 70 \text{ m}$) upon the normalized SO EsCB index for **a** total planetary

waves, **b** planetary wave 1 and **c** planetary wave 2. **b–d** As in **(a–c)**, but for the simulated results between sensitivity and control experiments. Dots for shadings indicate the 90% confidence level. Vectors only depict the part exceeding $10^5 \text{ m}^2 \text{ s}^{-2}$

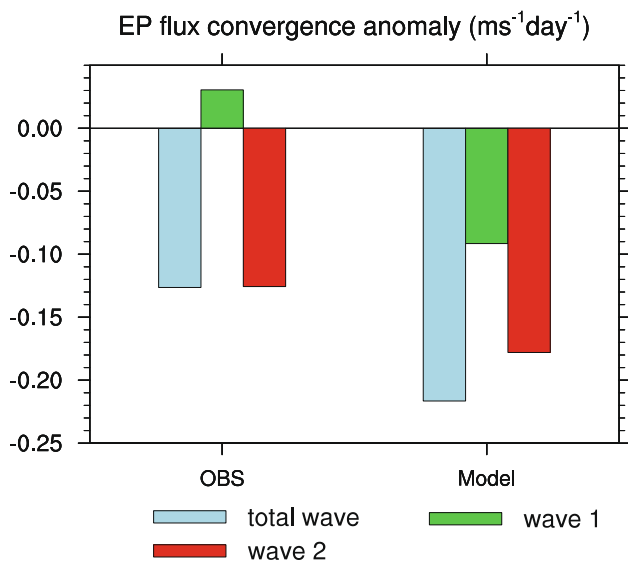
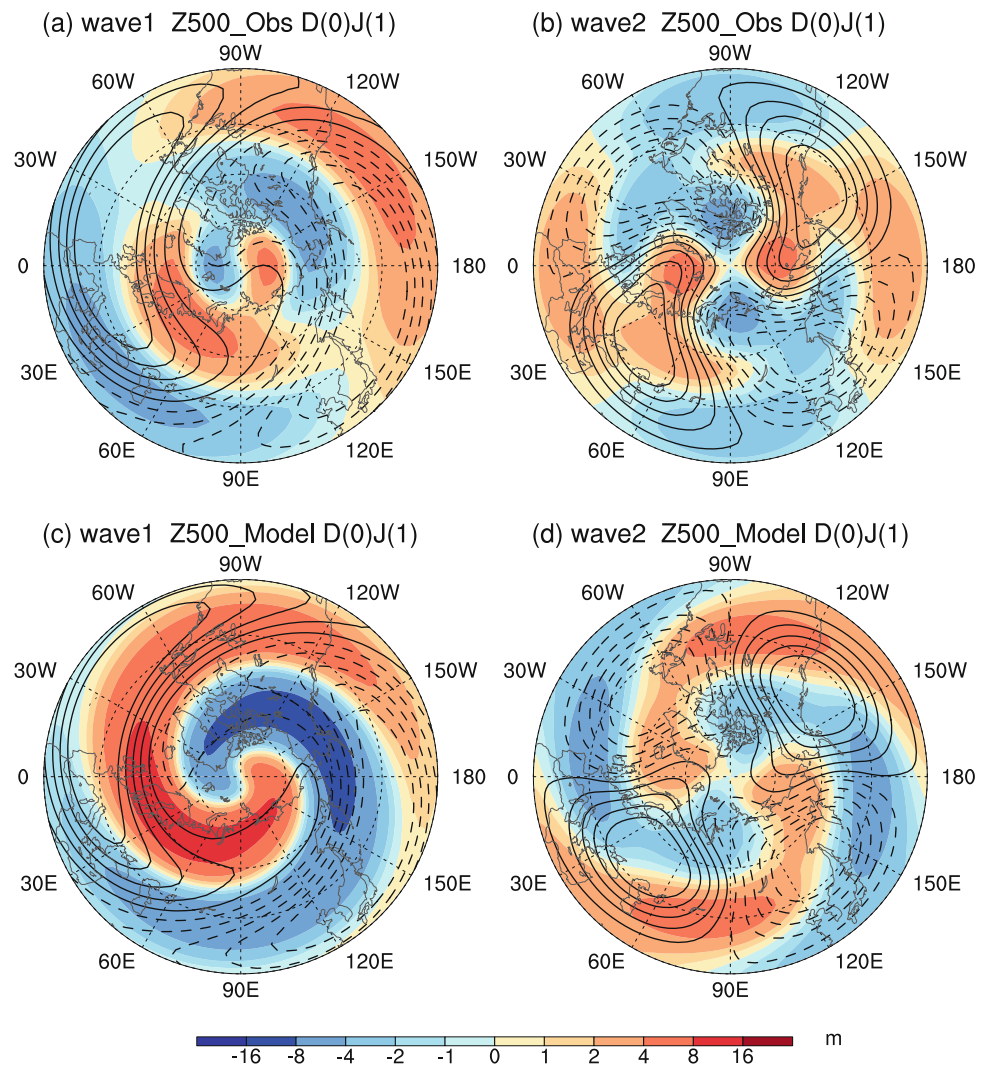


Fig. 8 Regressed and simulated results of area-mean EP flux convergence anomaly in the mid-high latitudes of lower stratosphere (100 hPa–30 hPa, $60^\circ\text{--}80^\circ \text{ N}$)

The above analyses reveal that the EsCB sea-ice sensitivity experiments well reproduce the main characteristics of the physical processes that involve the stratospheric pathway in the observations. However, certain simulation deviations still exist and should be noted. The simulated upward EP flux of planetary wave 2 is enhanced around 70° N and expands from the middle troposphere to the lower stratosphere (Fig. 7f). It shifts northward by about 10° and induces a stronger EP flux convergence anomaly than the observed branch (Fig. 7c). This deviation may be ascribed into a decrease in the amplitude of simulated planetary wave 2 around 60° N (Figs. 9d, 10d) instead of an increase in the observed amplitude (Figs. 9b, 10b). In addition, the enhancement of upward propagating planetary wave 1 around 50° N is also much stronger in the simulations (Fig. 7e) than that in the observations (Fig. 7b) because of the larger increased amplitude for the former (Figs. 9c, 10c). This possibly overestimates the contribution of planetary wave 1 to weakening of the lower stratospheric polar vortex in the simulations, featured by stronger EP flux convergence anomaly (Fig. 8). Several factors may be responsible for the above simulation deviations, such as the physical description of sea ice change, the initial atmospheric condition, the internal atmospheric variability and the height of the model top. In our design

Fig. 9 Regressed DJ geopotential height anomalies (shadings; unit: m) at 500 hPa of **a** planetary wave 1 and **b** planetary wave 2 upon normalized SO EsCB index. **c**, **d** as in (**a**, **b**), but for the simulated results between sensitivity and control experiments



for sensitivity experiment, only EsCB SIC from August to October is modified and then run for 80 years. The late summer initial atmospheric conditions are self-running, rather than particular atmospheric circulation anomalies that match SO EsCB sea ice loss in the observations. Different initial atmospheric conditions will affect the climate responses to reduced EsCB sea ice (Wu et al. 2017) and partly explain the simulation deviations. However, it does not change the main conclusion of our study and confirms the importance of Arctic sea ice in the Eurasian climate in turn. The height of the model top also affects the simulated performance of the stratospheric atmospheric circulation. For example, the high-top models exhibit an improved simulation skill for the quasi-biennial oscillation (QBO) in the tropical stratosphere and sudden stratospheric warming (SSW) occurrence in midwinter than the low-top models (Osprey et al. 2013; Palmeiro et al. 2020). As for atmospheric variability in the lower-middle stratosphere, both high-top and low-top models have a proper simulation (Palmeiro et al. 2020). Therefore,

considering that the stratospheric pathway mainly involves the lower-middle stratosphere (up to 10 hPa) and the limited computing resources in our analyses, CAM4 is sufficient to investigate the stratosphere-troposphere coupling and well capture the main physical processes seen in the observations though this low-top model will bring a few simulation deviations. Another reason for the simulation deviations may be derived from other external forcings because we cannot entirely exclude their nonlinear role in interfering with the linear regressed results.

5 Discussion

Previous sections have identified an intimate physical connection between early autumn sea ice anomaly in the EsCB Seas and early spring Ts variability over northern Eurasia, especially in central Russia, via generating anomalous upward propagating quasi-stationary planetary waves and

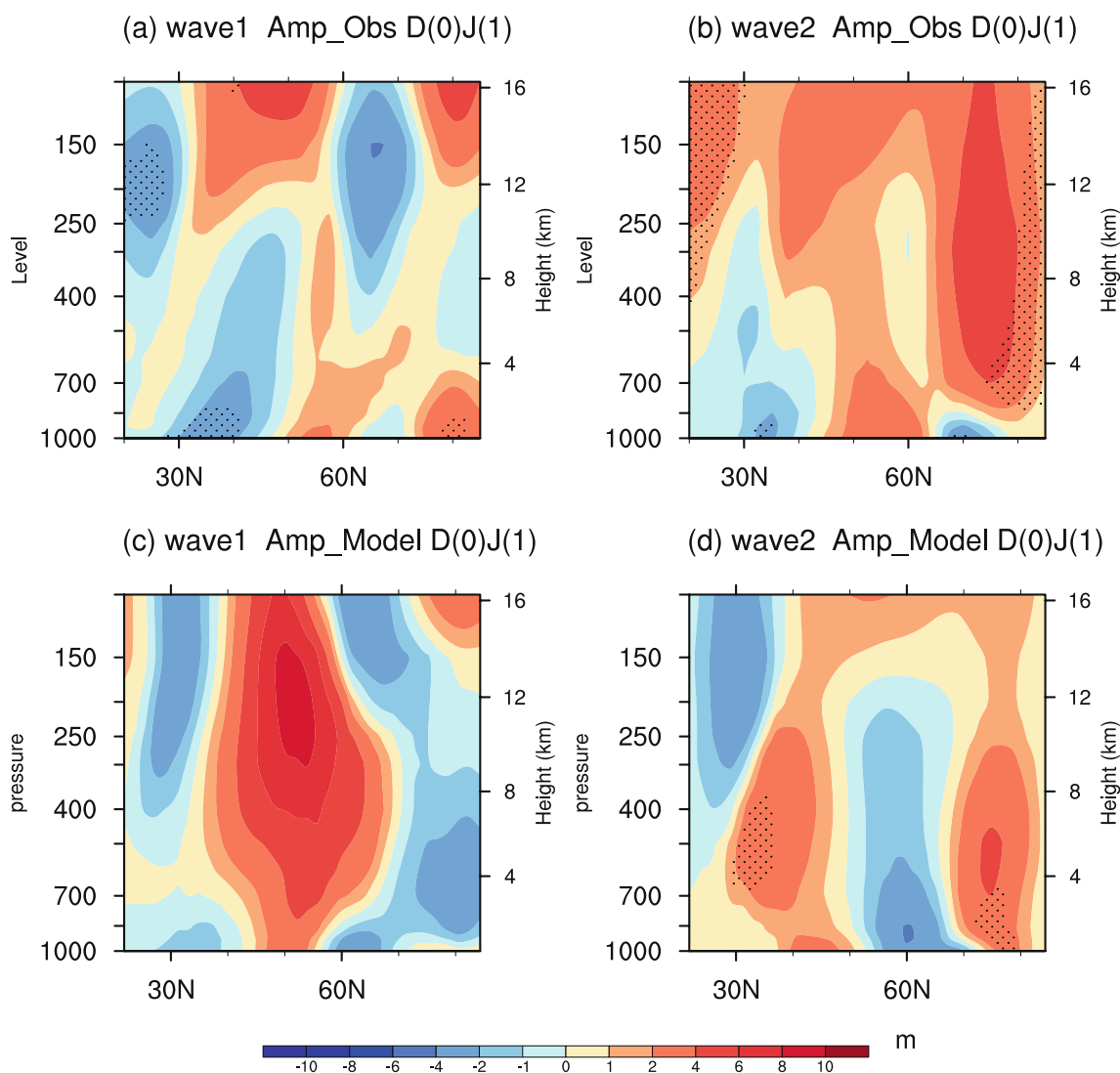


Fig. 10 Regressed DJ amplitude anomaly (shadings; unit: m) of **a** planetary wave 1 and **b** planetary wave 2 upon normalized SO EsCB index. **c**, **d** as in (**a**, **b**), but for the simulated results between sensitivity and control experiments

subsequently weakening the stratospheric polar vortex in winter. Here, a statistical prediction model is further designed to predict the early spring T_{RUS} index by utilizing the constructed early autumn EsCB index as the predictor in a linear regression equation. We use leave-one-out cross-validation to measure the potential predictability of this empirical model (Ham et al. 2013; Zuo et al. 2016; Chen and Wu 2018). A cross-validated correlation between the prediction and observation is then calculated as the skill score for assessing this empirical model's performance. When using the SO EsCB index to hindcast the MA T_{RUS} index, the cross-validated correlation is 0.41 and passes through 95% confidence level, indicating a considerable skill in the empirical prediction of early spring Ts variability in central Russia from early autumn EsCB sea ice anomaly. However, the predictive ability of an individual predictor is

limited because the early spring Ts variability over northern Eurasia is not only affected by the early autumn Arctic sea ice anomaly but also by other factors, such as ENSO, North Atlantic sea surface temperature anomalies, Eurasian snow cover, the internal atmospheric variability (AO/NAO), etc. For example, the perturbation of the JF stratospheric polar vortex is vital for the MA northern Eurasian climate change, and only part of its variations are linearly correlated to SO EsCB sea ice anomaly. Consequently, we subtract SO EsCB sea ice-related signals from the JF SPV index utilizing linear regression and extract the residual SPV index that is linearly uncorrelated with the EsCB index to represent the role of some other factors. After adding the JF residual SPV index to the empirical model as another predictor, the cross-validated correlation improves to 0.59, which is higher than only using SO EsCB index or JF residual SPV index. It also

implies that the early autumn EsCB sea ice indeed provides valid information to predict the early spring northern Eurasian Ts.

When SO EsCB sea ice reduces, more quasi-stationary planetary waves propagate into the lower stratosphere and result in the weakening of the winter polar vortex, which is possibly caused by the in-phase resonance of planetary waves and an increase in amplitude. In particular, the planetary wave 2 has played the primary role and its increased amplitude of geopotential height anomaly in the Arctic region (north of 60° N) can even be traced back to ON, lagging the decreased signal of sea ice in the EsCB Seas by 1 month. Although this indicates an intimate connection between SO EsCB sea ice decrease and the in-phase resonance of planetary wave 2 1 month later, the associated physical processes are not very clear. The lower tropospheric temperature anomalies of planetary wave 2 and anomalous net surface heat flux are then examined to discuss this question. The decrease of SO EsCB sea ice broadens the open water and induces local significant positive net surface heat flux anomaly based on the observations, justly corresponding to sea ice loss and occupying most regions of the Arctic Ocean (Fig. 11e). In the simulations, the distribution of net surface heat flux anomalies are approximately identical to the observations except for the negative anomaly to the north of the Canadian Archipelago, well capturing the significant positive anomaly from the Laptev Sea to the Beaufort Sea (Fig. 11f). It is likely attributed to the forcing of sea ice decrease is added merely to the EsCB Seas in the sensitivity experiment. This fan-shaped structure of more heat flux transport from the ocean to the atmosphere contributes to the lower tropospheric warming and the elevation of the Arctic geopotential height, creating the strongest anomalous center over the EsCB Seas (Fig. 11c, d). After operating the harmonic analysis, we found that the planetary wave 2 makes a dominant contribution to the Arctic atmospheric responses in the lower troposphere, especially for the warm and positive geopotential height anomalies over the EsCB Seas (Fig. 11a, b). The simulated results reproduce the main feature of the observed planetary wave 2 structure in the Arctic region, including evident warm (cold) anomalies over the EsCB Seas and the Greenland-Barents Seas (the Canadian Archipelago and the Kara-Laptev Seas). It is worth noting that the air temperature perturbation of planetary wave 2 can extend into the middle troposphere. This provides a few pieces of evidence to explain the possible mechanism for the generation of atmospheric anomalies of planetary wave 2 during a low EsCB sea ice. By contrast, for planetary wave 1, the ON air temperature anomalies covering the Arctic region are quite different in the observations and simulations, also corresponding to the distinct spatial structure of geopotential height anomalies (not shown). Until 2 months later, the observed and simulated geopotential height

anomalies gradually show similar signals, especially north of 60° N (Fig. 9a, c). It seemingly implies that the evolution of planetary wave 1 in the Arctic region is related to the reduced SO EsCB sea ice, but the notable simulation deviations in the first 2 months may be interfered with by the initial atmospheric condition. However, the above speculation still lacks enough support. The detailed dynamical or thermal connection between EsCB sea ice decrease and atmospheric anomalies of planetary waves 1–2 needs further analyses by sensitivity experiments and formula derivation.

The simulated results have demonstrated that the early autumn sea ice decrease in the EsCB Seas will lead to early spring evident cooling (multi-member mean) in central Russia and promote an increased occurrence probability of cold condition by about 30%. It does not mean there is no warm condition during low EsCB SIC year, but its occurrence probability has decreased according to the PDF of MA T_{RUS} index (Fig. 6a). This quasi-normal distribution of temperature anomaly may be related to the initial atmospheric condition or the internal atmospheric variability. Wu et al. (2017) emphasized the importance of summer Arctic atmospheric circulation conditions in strengthening negative feedback of Arctic sea ice decrease on the winter atmospheric circulation over Eurasia, generating a favorable atmospheric figuration that facilitates more frequent cold events. Thus, it is necessary to explore how different initial atmospheric conditions regulate the climate response of autumn ESCB sea ice loss in future work, which will contribute to improving the predictive ability.

Although observational studies and model experiments have shown the importance of Arctic sea ice in winter climate change in the northern hemisphere, some investigators still hold an opposite view and argued that there is little physical connection between reduced regional sea ice and cold winters across the mid-latitude continents (Barnes 2013; Chen et al. 2016a; McCusker et al. 2016; Sun et al. 2016; Collow et al. 2018; Blackport et al. 2019; Koenigk et al. 2019; Blackport and Screen 2020, 2021). The mid-latitude atmospheric circulation responses to the reduced Arctic sea ice are generally unstable and only exist under a few conditions (Chen et al. 2016a). Many simulated results also reported that Northern Hemispheric continental cooling and extreme cold events are probably attributed to the internal atmospheric variability, showing no or weak relations to the Arctic sea ice loss or Arctic amplification (Barnes 2013; McCusker et al. 2016; Smith et al. 2017; Collow et al. 2018; Koenigk et al. 2019; Blackport and Screen, 2020). Through separating the atmosphere forcing and the sea ice forcing, Blackport et al. (2019) further pointed out the warm Arctic-cold continents/Eurasia (WACC/E) is dominated by internal atmospheric dynamics while the influences of sea ice change are limited to the Arctic Ocean. Different approaches, models and experimental designs may obtain opposite results,

Fig. 11 **a** Regressed 1000 hPa air temperature (shadings; unit: °C) and 500 hPa geopotential height (contours; unit: m) anomalies in ON (October–November) of planetary wave 2 upon normalized SO EsCB index. **b** as in (a), but for the simulated results. **c, d** As in (a, b), respectively, but for the 1000 hPa air temperature (shadings; unit: °C) and 500 hPa geopotential height (contours; unit: m) anomalies. **e, f** As in (a, b), respectively, but for the net surface heat flux anomaly (shadings; unit: w m^{-2}). Dots for shadings indicate the 90% confidence level

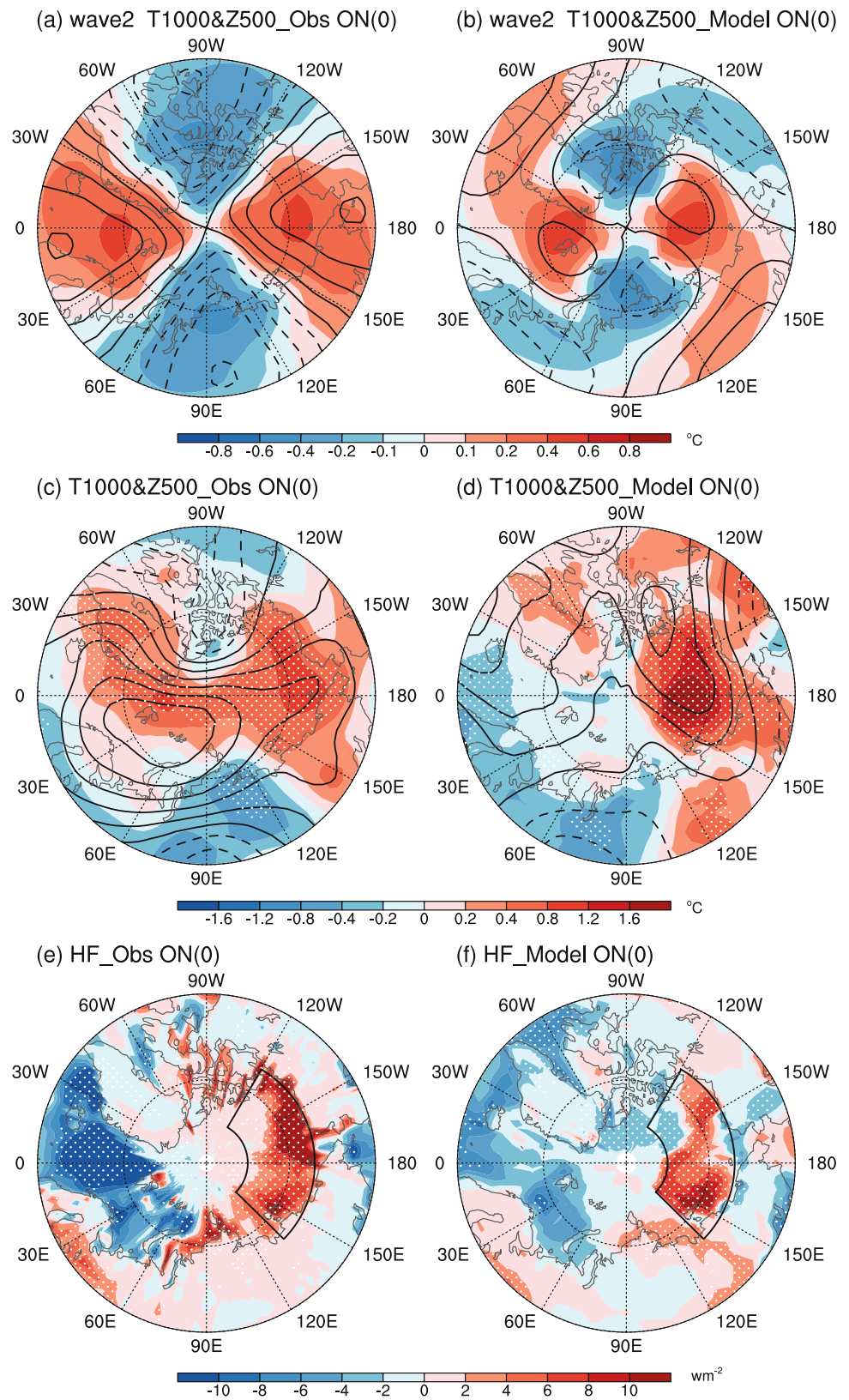
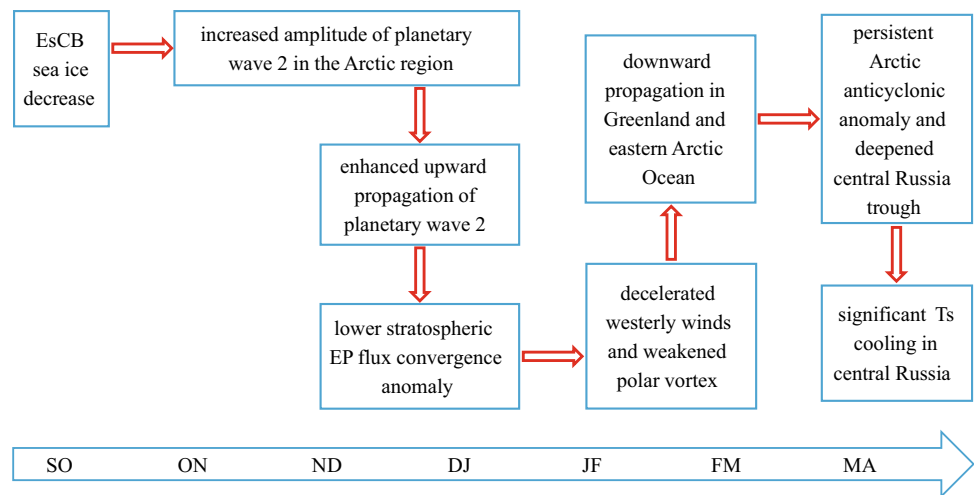


Fig. 12 Schematic diagram depicting the physical processes responsible for the influence of SO EsCB SIC on the subsequent early spring Eurasian Ts



thus more efforts should be paid to study the possible reasons for the uncertainty in the impacts of Arctic sea ice.

6 Summary

Based on the regressed analyses of reanalysis datasets (atmospheric variables from the NCEP-DOE Reanalysis II, SIC from the HADISST) and EsCB sea-ice sensitivity experiments, the present study reveals the significant impact of EsCB sea ice decrease in the early autumn on northern Eurasian cooling in the subsequent early spring at the interannual time scale, explaining approximately 25% Ts variation over central Russia ($r = -0.50$). The associated atmospheric anomalies are characterized by an anticyclonic anomaly covering the Arctic Ocean in the lower troposphere and a deepened trough over central Russia in the middle troposphere. The attenuation of the winter stratospheric polar vortex plays a crucial role in this cross-seasonal connection, and the detailed physical processes are summarized in the schematic diagram (Fig. 12). When the EsCB sea ice reduces (one interannual standard deviation) in the early autumn, significant warming and positive geopotential height anomaly occur in the Arctic region from lower to middle troposphere 1 month later, whose atmospheric perturbation is mainly dominated by planetary wave 2. The in-phase resonance of planetary wave 2 with its climatological mean is favorable for an increased amplitude in the troposphere and much more wave energy propagating into the lower stratosphere, manifested by anomalous upward propagation of EP flux. It will lead to EP flux convergence anomaly and decelerate the zonal westerly winds in JF, generating a weakened polar vortex in the lower stratosphere. Subsequently, the stratospheric signals with positive geopotential height anomalies propagate downward in the next 2 months and reach the troposphere in the early spring, especially around Greenland

and in the eastern Arctic Ocean. The former contributes to a zonal wave train propagating from the North Atlantic to eastern Eurasia, giving rise to a deepened trough over central Russia. And the latter maintains the Arctic anticyclonic anomaly and also contributes to the central Russian cyclonic anomaly. This anomalous atmospheric configuration in the lower-middle troposphere favors the southward intrusion of Arctic cold air along with the northerly winds, making central Russia experience a nearly 0.8 °C drop in the mean temperature and an increased occurrence probability of cold conditions by about 30%.

Acknowledgements This study is supported jointly by the Major Program of the National Natural Science Foundation of China (Grant 41790472), the National Natural Science Foundation of China (Grant 41905058), the State Key Program of National Natural Science of China (Grant 41730959), the National Key Basic Research Project of China (Grant 2019YFA0607002) and the National Science Foundation for Post-doctoral Scientists of China (Grant KLH1829028).

References

- Alexander MA, Bhatt US, Walsh JE, Timlin MS, Miller JS, Scott JD (2004) The atmospheric response to realistic Arctic sea-ice anomalies in an AGCM during winter. *J Clim* 17:890–905. [https://doi.org/10.1175/1520-0442\(2004\)017,0890:TARTRA.2.0.CO;2](https://doi.org/10.1175/1520-0442(2004)017,0890:TARTRA.2.0.CO;2)
- Ambaum MHP, Hoskins BJ (2002) The NAO troposphere-stratosphere connection. *J Clim* 15(14):1969–1978
- Andrews DG, Holton JR, Leovy CB (1987) *Middle atmosphere dynamics*. Academic Press, p 489
- Baldwin MP, Dunkerton TJ (2001) Stratospheric harbinger of anomalous weather regimes. *Science* 294:581–584
- Barnes EA (2013) Revisiting the evidence linking Arctic amplification to extreme weather in midlatitudes. *Geophys Res Lett* 40:4734–4739. <https://doi.org/10.1002/grl.50880>
- Blackport R, Kushner PJ (2017) Isolating the atmospheric circulation response to Arctic sea ice loss in the coupled climate system. *J Clim* 30:2163–2185. <https://doi.org/10.1175/JCLI16-0257.1>

- Blackport R, Screen JA (2020) Insignificant effect of Arctic amplification on the amplitude of midlatitude atmospheric waves. *Sci Adv* 6:eayy2880. <https://doi.org/10.1126/sciadv.aay2880>
- Blackport R, Screen JA (2021) Observed statistical connections overestimate the causal effects of Arctic Sea ice changes on midlatitude winter climate. *J Clim* 34(8):3021–3038
- Blackport R, Screen JA, van der Wiel K, Bintanja R (2019) Minimal influence of reduced Arctic sea ice on coincident cold winters in mid-latitudes. *Nat Clim Change* 9:697–704. <https://doi.org/10.1038/s41558-019-0551-4>
- Budikova D (2009) Role of Arctic sea ice in global atmospheric circulation: a review. *Glob Planet Change* 68:149–163. <https://doi.org/10.1016/j.gloplacha.2009.04.001>
- Castanheira JM, Liberato MLR, de la Torre L, Graf HF, DaCamara CC (2009) Baroclinic Rossby wave forcing and barotropic Rossby wave response to stratospheric vortex variability. *J Atmos Sci* 66:902–914. <https://doi.org/10.1175/2008JAS2862.1>
- Chen S, Wu R (2018) Impacts of early autumn Arctic sea ice concentration on subsequent spring Eurasian surface air temperature variations. *Clim Dyn* 51:2523–2542. <https://doi.org/10.1007/s00382-017-4026-x>
- Chen W, Graf HF, Takahashi M (2002) Observed interannual oscillations of planetary wave forcing in the Northern Hemisphere winter. *Geophys Res Lett* 29:2073. <https://doi.org/10.1029/2002GL016062>
- Chen W, Takahashi M, Graf HF (2003) Interannual variations of stationary planetary wave activity in the northern winter troposphere and stratosphere and their relations to NAM and SST. *J Geophys Res* 108:4797. <https://doi.org/10.1029/2003JD003834>
- Chen S, Chen W, Wei K (2013) Recent trends in winter temperature extremes in eastern China and their relationship with the Arctic Oscillation and ENSO. *Adv Atmos Sci* 30:1712–1724. <https://doi.org/10.1007/s00376-013-2296-8>
- Chen Z, Wu R, Chen W (2014) Impacts of autumn Arctic sea ice concentration changes on the East Asian winter monsoon variability. *J Clim* 27:5433–5450. <https://doi.org/10.1175/JCLI-D-13-00731.1>
- Chen HW, Zhang F, Alley RB (2016a) The robustness of midlatitude weather pattern changes due to Arctic sea ice loss. *J Clim* 29:7831–7849. <https://doi.org/10.1175/JCLI-D-16-0167.1>
- Chen HW, Alley RB, Zhang F (2016b) Interannual Arctic sea ice variability and associated winter weather patterns: a regional perspective for 1979–2014. *J Geophys Res Atmos* 121(14):433–455. <https://doi.org/10.1002/2016JD024769>
- Chen S, Wu R, Chen W, Song L, Cheng W, Shi W (2021) Weakened impact of autumn Arctic sea ice concentration change on the subsequent winter Siberian High variation around the late-1990s. *Int J Climatol* 41:E2700–E2717
- Cohen J, Barlow M, Kushner PJ, Saito K (2007) Stratosphere–troposphere coupling and links with Eurasian land surface variability. *J Clim* 20:5335–5343. <https://doi.org/10.1175/2007JCLI1725.1>
- Cohen J, Pfeiffer K, Francis J (2018) Warm Arctic episodes linked with increased frequency of extreme winter weather in the United States. *Nat Commun* 9:869. <https://doi.org/10.1038/s41467-018-02992-9>
- Cohen J, Zhang X, Francis J et al (2020) Divergent consensus on Arctic amplification influence on midlatitude severe winter weather. *Nat Climate Change* 10:20–29. <https://doi.org/10.1038/s41558-019-0662-y>
- Coles S (2001) An introduction to statistical modeling of extreme values. Springer, p 208
- Collow TW, Wang W, Kumar A (2018) Simulations of Eurasian winter temperature trends in coupled and uncoupled CFSv2. *Adv Atmos Sci* 35:14–26. <https://doi.org/10.1007/s00376-017-6294-0>
- Deser C, Teng H (2013) Recent trends in Arctic sea ice and the evolving role of atmospheric circulation forcing, 1979–2007. In: Arctic Sea ice decline: observations, projections, mechanisms, and implications, *geophys monogr* Vol. 180. Amer Geophys Union, pp 7–26. <https://doi.org/10.1029/180GM03>
- Deser C, Walsh JE, Timlin MS (2000) Arctic sea ice variability in the context of recent atmospheric circulation trends. *J Clim* 13:617–633. [https://doi.org/10.1175/1520-0442\(2000\)013,0617:ASIVIT.2.0.CO;2](https://doi.org/10.1175/1520-0442(2000)013,0617:ASIVIT.2.0.CO;2)
- Deser C, Magnusdottir G, Saravanan R, Phillips A (2004) The effects of North Atlantic SST and sea-ice anomalies on the winter circulation in CCM3. Part II: direct and indirect components of the response. *J Clim* 17:877–889. [https://doi.org/10.1175/1520-0442\(2004\)017,0877:TEONAS.2.0.CO;2](https://doi.org/10.1175/1520-0442(2004)017,0877:TEONAS.2.0.CO;2)
- Deser C, Tomas R, Alexander M, Lawrence D (2010) The seasonal atmospheric response to projected Arctic sea ice loss in the late twenty-first century. *J Clim* 23:333–351. <https://doi.org/10.1175/2009JCLI3053.1>
- Dethloff K, Rinke A, Benkel A, Koltzow M, Stendel M (2006) A dynamical link between the Arctic and the global climate system. *Geophys Res Lett* 33:L03703. <https://doi.org/10.1029/2005GL025245>
- Ding S, Chen W, Feng J, Graf HF (2017) Combined impacts of PDO and two types of La Niña on climate anomalies in Europe. *J Climate* 30(9):3253–3278. <https://doi.org/10.1175/JCLI-D-16-0376.1>
- Ding S, Chen W, Graf HF, Guo Y, Nath D (2018) Distinct winter patterns of tropical Pacific convection anomaly and the associated extratropical wave trains in the Northern Hemisphere. *Clim Dyn* 51(5–6):2003–2022
- Ding S, Wu B, Chen W (2021) Dominant Characteristics of early autumn Arctic sea ice variability and its impact on Winter Eurasian climate. *J Clim* 34(5):1825–1846
- Edmon H, Hoskins BJ, McIntyre ME (1980) Eliassen–Palm cross sections for the troposphere. *J Atmos Sci* 37:2600–2616. [https://doi.org/10.1175/1520-0469\(1980\)037,2600:EPCSFT.2.0.CO;2](https://doi.org/10.1175/1520-0469(1980)037,2600:EPCSFT.2.0.CO;2)
- Efron B, Tibshirani RJ (1994) An Introduction to the Bootstrap. Chapman and Hall, p 456
- Francis JA, Vavrus SJ (2012) Evidence linking Arctic amplification to extreme weather in mid-latitudes. *Geophys Res Lett* 39:L06801. <https://doi.org/10.1029/2012GL051000>
- Francis JA, Vavrus SJ (2015) Evidence for a wavier jet stream in response to rapid Arctic warming. *Environ Res Lett* 10:014005. <https://doi.org/10.1088/1748-9326/10/1/014005>
- Francis JA, Chan W, Leathers DJ, Miller JR, Veron DE (2009) Winter Northern Hemisphere weather patterns remember summer Arctic sea-ice extent. *Geophys Res Lett* 36:L07503. <https://doi.org/10.1029/2009GL037274>
- Gao Y, Sun J, Li F, He S, Suo L (2015) Arctic sea ice and Eurasian climate: review. *Adv Atmos Sci* 32:92–114. <https://doi.org/10.1007/s00376-014-0009-6>
- Garfinkel CI, Waugh DW, Gerber EP (2013) The effect of tropospheric jet latitude on coupling between the stratospheric polar vortex and the troposphere. *J Climate* 26:2077–2095. <https://doi.org/10.1175/JCLI-D-12-00301.1>
- Graf HF, Zanchettin D (2012) Central Pacific El Niño, the “subtropical bridge”, and Eurasian climate. *J Geophys Res* 117(D1):D01102. <https://doi.org/10.1029/2011JD016493>
- Graf HF, Davide Z, Claudia T, Matthias B (2014) Observational constraints on the tropospheric and near surface winter signature of the Northern Hemisphere stratospheric polar vortex. *Clim Dyn* 43:3245–3266. <https://doi.org/10.1007/s00382-014-2101-0>
- Gu S, Zhang Y, Wu Q, Yang X (2018) The linkage between arctic sea ice and midlatitude weather: In the perspective of energy. *J Geophys Res Atmos* 123(11):536–550. <https://doi.org/10.1029/2018JD028743>

- Ham YG, Kug JS, Park JY, Jin F (2013) Sea surface temperature in the north tropical Atlantic as a trigger for El Niño/Southern Oscillation events. *Nat Geosci* 6:112–116
- Honda M, Inoue J, Yamane S (2009) Influence of low Arctic sea-ice minima on anomalously cold Eurasian winters. *Geophys Res Lett* 36:L08707. <https://doi.org/10.1029/2008GL037079>
- Hopsch S, Cohen J, Dethloff K (2012) Analysis of a link between fall Arctic sea ice concentration and atmospheric patterns in the following winter. *Tellus* 64A:18624. <https://doi.org/10.3402/tellusa.v64i0.18624>
- Inoue J, Hori ME, Takaya K (2012) The role of Barents Sea ice in the wintertime cyclone track and emergence of a warm-Arctic cold-Siberian anomaly. *J Clim* 25:2561–2568. <https://doi.org/10.1175/JCLI-D-11-00449.1>
- Ionita M, Lohmann G, Rimbu N, Scholz P (2012) Dominant modes of diurnal temperature range variability over Europe and their relationships with large-scale atmospheric circulation and sea surface temperature anomaly patterns. *J Geophys Res* 117:D15111. <https://doi.org/10.1029/2011JD016669>
- Jaiser R, Dethloff K, Handorf D, Rinke A, Cohen J (2012) Impact of sea ice cover changes on the Northern Hemisphere atmospheric winter circulation. *Tellus* 64A:11595. <https://doi.org/10.3402/tellusa.v64i0.11595>
- Jaiser R, Dethloff K, Handorf D (2013) Stratospheric response to Arctic sea ice retreat and associated planetary wave propagation changes. *Tellus A Dyn Meteorol Oceanogr* 65(1):19375. <https://doi.org/10.3402/tellusa.v65i0.19375>
- Kanamitsu M, Ebisuzaki W, Woollen J, Yang SK, Hnilo JJ, Fiorino M, Potter GL (2002) NCEP-DOE AMIP-II Reanalysis (R-2). *Bull Amer Meteorol Soc* 83:1631–1643. <https://doi.org/10.1175/BAMS-83-11-1631>
- Kim HJ, Ahn JB (2012) Possible impact of the autumnal North Pacific SST and November AO on the East Asian winter temperature. *J Geophys Res* 117:D12104. <https://doi.org/10.1029/2012JD017527>
- King MP, Hell M, Keenlyside N (2015) Investigation of the atmospheric mechanisms related to the autumn sea ice and winter circulation link in the Northern Hemisphere. *Clim Dyn* 46:1185–1195. <https://doi.org/10.1007/s00382-015-2639-5>
- Koenigk T, Gao Y, Gastineau G et al (2019) Impact of Arctic sea ice variations on winter temperature anomalies in Northern Hemisphere land areas. *Climate Dyn* 52:3111–3137. <https://doi.org/10.1007/s00382-018-4305-1>
- Kug JS, Jeong JH, Jang YS, Kim BM, Folland CK, Min SK, Son SW (2015) Two distinct influences of Arctic warming on cold winters over North America and East Asia. *Nat Geosci* 8:759–762. <https://doi.org/10.1038/ngeo2517>
- Li M, Luo D, Simmonds I, Dai A, Zhong L, Yao Y (2021) Anchoring of atmospheric teleconnection patterns by Arctic sea ice loss and its link to winter cold anomalies in East Asia. *Int J Climatol* 41(1):547–558
- Magnusdottir G, Deser C, Saravanan R (2004) The effects of North Atlantic SST and sea-ice anomalies on the winter circulation in CCM3. Part I: main features and storm track characteristics of the response. *J Clim* 17:857–876. [https://doi.org/10.1175/1520-0442\(2004\)017<0857:TEONAS.2.0.CO;2](https://doi.org/10.1175/1520-0442(2004)017<0857:TEONAS.2.0.CO;2)
- McCusker KE, Fyfe JC, Sigmund M (2016) Twenty-five winters of unexpected Eurasian cooling unlikely due to Arctic sea-ice loss. *Nat Geosci* 9:838–842. <https://doi.org/10.1038/ngeo2820>
- Michailidis G, Stoev S (2012) Extreme value theory: an introduction. *Technometrics* 49(4):491–492
- Miyazaki C, Yasunari T (2008) Dominant interannual and decadal variability of winter surface air temperature over Asia and the surrounding oceans. *J Climate* 21:1371–1386. <https://doi.org/10.1175/2007JCLI1845.1>
- Mori M, Watanabe M, Shiogama H, Inoue J, Kimoto M (2015) Robust Arctic sea-ice influence on the frequent Eurasian cold winters in past decades. *Nat Geosci* 7:869–873. <https://doi.org/10.1038/ngeo2277>
- Mori M, Kosaka Y, Watanabe M, Nakamura H, Kimoto M (2019) A reconciled estimate of the influence of Arctic sea-ice loss on recent Eurasian cooling. *Nat Clim Change* 9:123–129. <https://doi.org/10.1038/s41558-018-0379-3>
- Mudelsee M (2010) Climate time series analysis: classical statistical and bootstrap methods. Springer, p 474. <https://doi.org/10.1007/978-90-481-9482-7>
- Nakamura T, Yamazaki K, Iwamoto K, Honda M, Miyoshi Y, Ogawa Y, Ukita J (2015) A negative phase shift of the winter AO/NAO due to the recent Arctic sea-ice reduction in late autumn. *J Geophys Res Atmos* 120:3209–3227. <https://doi.org/10.1002/2014JD022848>
- Nakamura T, Yamazaki K, Sato T, Ukita J (2019) Memory effects of Eurasian land processes cause enhanced cooling in response to sea ice loss. *Nat Commun* 10:5111. <https://doi.org/10.1038/s41467-019-13124-2>
- Neale RB, et al (2010) Description of the NCAR Community Atmosphere Model (CAM 4.0). NCAR Tech. Note NCAR/TN-4851STR, p 212
- Ogawa F, Keenlyside N, Gao Y, Koenigk T, Yang S, Suo L, Wang T, Gastineau G, Nakamura T, Cheung HN (2018) Evaluating impacts of recent Arctic sea ice loss on the Northern Hemisphere winter climate change. *Geophys Res Lett* 45:3255–3263. <https://doi.org/10.1002/2017GL076502>
- Orsolini YJ, Senan R, Benestad RE, Melsom A (2012) Autumn atmospheric response to the 2007 low Arctic sea ice extent in coupled ocean–atmosphere hindcasts. *Clim Dyn* 38:2437–2448. <https://doi.org/10.1007/s00382-011-1169-z>
- Osprey SM, Gray LJ, Hardiman SC, Butchart N, Hinton TJ (2013) Stratospheric variability in twentieth-century CMIP5 simulations of the Met Office climate model: High top versus low top. *J Clim* 26:1595–1606. <https://doi.org/10.1175/JCLI-D-12-00147.1>
- Overland JE, Wang M (2018) Resolving future Arctic/midlatitude weather connections. *Earth's Future* 6:1146–1152. <https://doi.org/10.1029/2018EF000901>
- Overland JE, Ballinger TJ, Cohen J et al (2021) How do intermittency and simultaneous processes obfuscate the Arctic influence on midlatitude winter extreme weather events? *Environ Res Lett* 16:043002. <https://doi.org/10.1088/1748-9326/abdb5d>
- Palmeiro FM, García-Serrano J, Bellprat O, Bretonnière PA, Doblas-Reyes FJ (2020) Boreal winter stratospheric variability in EC-EARTH: High-top versus low-top. *Clim Dyn* 54:3135–3150. <https://doi.org/10.1007/s00382-020-05162-0>
- Pedersen RA, Cvijanovic I, Langen PL, Vinther BM (2016) The impact of regional Arctic sea ice loss on atmospheric circulation and the NAO. *J Clim* 29:889–902. <https://doi.org/10.1175/jcli-d-15-0315.1>
- Petoukhov V, Semenov V (2010) A link between reduced Barents-Kara sea ice and cold winter extremes over northern continents. *J Geophys Res* 115:D21111. <https://doi.org/10.1029/2009JD013568>
- Plumb RA (1985) On the three-dimensional propagation of stationary waves. *J Atmos Sci* 42:217–229. [https://doi.org/10.1175/1520-0469\(1985\)042<0217:OTTDPO.2.0.CO;2](https://doi.org/10.1175/1520-0469(1985)042<0217:OTTDPO.2.0.CO;2)
- Rayner NA, Parker DE, Horton EB, Folland CK, Alexander LV, Rowell DP, Kent EC, Kaplan A (2003) Global analyses of sea surface temperature, sea ice, and night marine air temperature since the late nineteenth century. *J Geophys Res* 108:4407. <https://doi.org/10.1029/2002JD002670>
- Rinke A, Dethloff K, Dorn W, Handorf D, Moore JC (2013) Simulated Arctic atmospheric feedbacks associated with late summer sea ice anomalies. *J Geophys Res Atmos* 118:7698–7714. <https://doi.org/10.1002/jgrd.50584>

- Scaife AA, Spanghel T, Fereday DR et al (2012) Climate change projections and stratosphere–troposphere interaction. *Clim Dyn* 38:2089–2097. <https://doi.org/10.1007/s00382-011-1080-7>
- Screen JA (2017) Simulated atmospheric response to regional and pan-Arctic sea ice loss. *J Clim* 30:3945–3962. <https://doi.org/10.1175/JCLI-D-16-0197.1>
- Screen JA, Simmonds I (2010) The central role of diminishing sea ice in recent Arctic temperature amplification. *Nature* 464:1334–1337. <https://doi.org/10.1038/nature09051>
- Serreze MC, Holland MM, Stroeve J (2007) Perspectives on Arctic's shrinking sea-ice cover. *Science* 315:1533–1536. <https://doi.org/10.1126/science.1139426>
- Singarayer JS, Valdes PJ, Bamber JL (2005) The atmospheric impact of uncertainties in recent Arctic sea-ice reconstructions. *J Clim* 18:3996–4012. <https://doi.org/10.1175/JCLI3490.1>
- Smith DM, Dunstone NJ, Scaife AA, Fiedler EK, Copsey D, Hardiman SC (2017) Atmospheric response to Arctic and Antarctic sea ice: the importance of ocean-atmosphere coupling and the background state. *J Clim* 30:4547–4565
- Song L, Wu R (2019a) Different cooperation of the Arctic Oscillation and the Madden-Julian oscillation in the East Asian cold events during early and late winter. *J Geophys Res Atmos* 124:4913–4931
- Song L, Wu R (2019b) Precursory signals of East Asian winter cold anomalies in stratospheric planetary wave pattern. *Clim Dyn* 52:5965–5983
- Sun L, Perlwitz J, Hoerling M (2016) What caused the recent “warm Arctic, cold continents” trend pattern in winter temperatures? *Geophys Res Lett* 43:5345–5352. <https://doi.org/10.1002/2016GL069024>
- Takaya K, Nakamura H (1997) A formulation of a wave activity flux for stationary Rossby waves on a zonally varying basic flow. *Geophys Res Lett* 24:2985–2988. <https://doi.org/10.1029/97GL03094>
- Takaya K, Nakamura H (2001) A formulation of a phase-independent wave-activity flux for stationary and migratory quasi-geostrophic eddies on a zonally varying basic flow. *J Atmos Sci* 58:608–627. [https://doi.org/10.1175/1520-0469\(2001\)058<0608:AFOAPI.2.0.CO;2](https://doi.org/10.1175/1520-0469(2001)058<0608:AFOAPI.2.0.CO;2)
- Tang QH, Zhang X, Yang X, Francis JA (2013) Cold winter extremes in northern continents linked to Arctic sea ice loss. *Environ Res Lett* 8:014036. <https://doi.org/10.1088/1748-9326/8/1/014036>
- Vihma T (2014) Effects of Arctic sea ice decline on weather and climate: a review. *Surv Geophys* 35:1175–1214. <https://doi.org/10.1007/s10712-014-9284-0>
- Vihma T, Graverson R, Chen L, Handorf D, Skific N, Francis JA, Tyrrell N, Hall R, Hanna E, Uotila P (2020) Effects of the tropospheric large-scale circulation on European winter temperatures during the period of amplified Arctic warming. *Int J Climatol* 40:509–529. <https://doi.org/10.1002/joc.6225>
- Wu R, Chen S (2016) Regional change in snow water equivalent–surface air temperature relationship over Eurasia during boreal spring. *Clim Dyn* 47:2425–2442. <https://doi.org/10.1007/s00382-015-2972-8>
- Wu B, Huang R, Gao D (1999) Effects of variation of winter sea-ice area in Kara and Barents seas on East Asia winter monsoon. *Acta Meteorol Sin* 13:141–153
- Wu R, Yang S, Liu S, Sun L, Lian Y, Gao Z (2010) Changes in the relationship between Northeast China summer temperature and ENSO. *J Geophys Res* 115:D21107. <https://doi.org/10.1029/2010JD014422>
- Wu B, Su J, Zhang R (2011a) Effects of autumn–winter Arctic sea ice on winter Siberian high. *Chin Sci Bull* 56:3220–3228. <https://doi.org/10.1007/s11434-011-4696-4>
- Wu R, Yang S, Liu S, Sun L, Lian Y, Gao Z (2011b) Northeast China summer temperature and North Atlantic SST. *J Geophys Res* 116:D16116. <https://doi.org/10.1029/2011JD015779>
- Wu B, Handorf D, Dethloff K, Rinke A, Hu A (2013) Winter weather patterns over northern Eurasia and Arctic sea ice loss. *Mon Wea Rev* 141:3786–3800. <https://doi.org/10.1175/MWR-D-13-00046.1>
- Wu R, Zhao P, Liu G (2014) Change in the contribution of spring snow cover and remote oceans to summer air temperature anomaly over Northeast China around 1990. *J Geophys Res* 119:663–676
- Wu B, Su J, D'Arrigo R (2015) Patterns of Asian winter climate variability and links to Arctic sea ice. *J Climate* 28:6841–6857
- Wu Z, Li X, Li YJ, Li Y (2016) Potential influence of Arctic sea ice to the interannual variations of East Asian spring precipitation. *J Climate* 29:2797–2813
- Wu B, Yang K, Francis JA (2017) A cold event in Asia during January–February 2012 and its possible association with arctic sea ice loss. *J Climate* 30:7971–7990. <https://doi.org/10.1175/JCLI-D-16-0115.1>
- Xu M, Tian W, Zhang J, Wang T, Qie K (2021) Impact of Sea Ice Reduction in the Barents and Kara Seas on the Variation of the East Asian Trough in Late Winter. *J Climate* 34(3):1081–1097
- Ye K, Wu R, Liu Y (2015) Interdecadal change of Eurasian snow, surface temperature, and atmospheric circulation in the late 1980s. *J Geophys Res* 120:2738–2753. <https://doi.org/10.1002/2015JD023148>
- Zhang P, Wu Y, Smith KL (2018a) Prolonged effect of the stratospheric pathway in linking Barents-Kara Sea sea ice variability to the midlatitude circulation in a simplified model. *Climatol Dyn* 50:527–539. <https://doi.org/10.1007/s00382-017-3624-y>
- Zhang P, Wu Y, Simpson IR, Smith KL, Zhang X, De B, Callaghan P (2018b) A stratospheric pathway linking a colder Siberia to Barents-Kara Sea sea ice loss. *Sci Adv* 4:eaat6025. <https://doi.org/10.1126/sciadv.aat6025>
- Zuo J, Ren H, Wu B, Li W (2016) Predictability of winter temperature in China from previous autumn Arctic sea ice. *Climatol Dyn* 47:2331–2343
- Zveryaev II, Gulev SK (2009) Seasonality in secular changes and interannual variability of European air temperature during the twentieth century. *J Geophys Res* 114:D02110. <https://doi.org/10.1029/2008JD010624>

Publisher's Note Springer Nature remains neutral with regard to jurisdictional claims in published maps and institutional affiliations.